

## Article

# Evaluation of the Acceleration Vibration Signal for Aggregates of the Horizontal Drilling Stand

Patrik Flegner <sup>\*</sup>, Ján Kačur , Milan Durdán  and Marek Laciak 

Institute of Control and Informatization of Production Processes, Faculty BERG, Technical University of Košice, Némcevej 3, 042 00 Košice, Slovakia; jan.kacur@tuke.sk (J.K.); milan.durdan@tuke.sk (M.D.); marek.laciak@tuke.sk (M.L.)

\* Correspondence: patrik.flegner@tuke.sk; Tel.: +421-55-602-5174

**Featured Application:** In the presented research, methods of processing the vibrational signal of acceleration from horizontal drilling rig aggregates were applied. The significance of the given study is that signal processing methods have not yet been applied to such an extent, despite the fact that the mining industry requires them. The presented significant results will help streamline the drilling process and prevent machinery accidents. Reference operating modes have been investigated and designed to determine vibrational statistical characteristics, autocorrelation functions, spectra, and spectrograms. Their research will help locate sources of strong unwanted vibrations.

**Abstract:** During the operation of each machine, there are dynamic effects causing vibrations. Such a device is also an experimental horizontal drilling stand with aggregates, i.e., a direct current motor (DC), a pump, and a hydro-generator. During their operation, unwanted vibration acceleration signals are generated. It is clear that the accompanying vibration signal carries integrating information about the current state of the drilling rig. Vibration signal processing methods for the time and frequency domains were used. The results of time-domain processing showed significant differences in time waveforms, statistical characteristics, and auto-correlation functions. The auto-correlation function pointed to the periodicity and dependence of the vibrational signal samples. Based on the acquired knowledge, the signals were classified, and a strong source of vibration was determined. Noise is superimposed on the harmonic components of the signals. Amplitude and power spectra were constructed in the frequency domain. Dominant frequencies were identified for each investigated mode in the operating mode. Power spectra removed less significant frequencies and focused on the dominant ones. Time-frequency spectrograms revealed significantly higher frequency bands. The proposed methods can be implemented in diagnosing the operation of the machine and aggregates, determining the source of the greatest vibrations, wear of parts of the equipment such as the drill bit, and recognition of the overall condition of the equipment.

**Keywords:** vibration response; horizontal drilling stand; time-frequency analysis; acceleration; mode parameter; rock disintegration; mode parameters; acceleration vibration; spectrum; spectrogram



**Citation:** Flegner, P.; Kačur, J.; Durdán, M.; Laciak, M. Evaluation of the Acceleration Vibration Signal for Aggregates of the Horizontal Drilling Stand. *Appl. Sci.* **2022**, *12*, 3984. <https://doi.org/10.3390/app12083984>

Academic Editor: Arcady Dyskin

Received: 25 February 2022

Accepted: 12 April 2022

Published: 14 April 2022

**Publisher's Note:** MDPI stays neutral with regard to jurisdictional claims in published maps and institutional affiliations.



**Copyright:** © 2022 by the authors. Licensee MDPI, Basel, Switzerland. This article is an open access article distributed under the terms and conditions of the Creative Commons Attribution (CC BY) license (<https://creativecommons.org/licenses/by/4.0/>).

## 1. Introduction

Rock disintegration by rotary drilling is one of the most important technological operations in the field of mining and mineral processing. If the disintegration process has to be effective, it needs to be monitored, optimized, and managed [1,2]. This requires the measurement of input process variables (such as pressure on the drilling tool  $F$  (N) and tool speed  $n$  (rpm)) as well as output variables (such as noise, vibration, and borehole length). An essential factor in this rotary rock disintegration technology is the interaction of the disintegrating tool with the disintegrated rock [3]. The interaction of the drilling tool with the rock is a source of vibrations and noise, the negative effects of which are

fundamentally reflected in the machinery [4,5]. Knowledge of the laws of origin and suppression of vibrations allows designers to design machines and equipment to effectively reduce the intensity of vibration during their operation and ensure smooth operation [6]. The operation of machinery and equipment should also include their continuous vibro-diagnostics combined with operation monitoring. Analytical, numerical, and experimental methods are currently used to solve vibration problems [7,8]. Although numerical methods are more often used in industrial practice, experimental analysis methods are in many cases the only possible way to determine real dynamic parameters [9,10]. Due to this, the drilling process is random, mainly due to the inhomogeneity of the drilled material. It is then clear that the measured oscillating movement of the drilling device is also random. Subsequently, the time-frequency analysis must be based on the statistical and frequency processing of the measured vibration response signal of the drilling stand [11–13]. In this case, the vibration response of the drilling device is the acceleration of the vibration movement in different operating modes. In the conditions of a laboratory experiment on a drilling stand, two basic states for vibrations can be distinguished:

- no-load vibration;
- vibrations during rotational disintegration of selected rocks.

Idle vibrations have the following components:

- vibrations from main aggregates;
- rinsing water vibrations.

The proposed signal processing methods will provide useful information in the vibro-diagnostics of the drilling equipment, followed by the current technological state of the equipment, as well as the time waveform of the technological process and operations [14–16].

## 2. Experiments Methodology—Description of the Drilling Stand

The research subject was a vibration signal generated by a laboratory horizontal drilling stand. The drilling stand was developed and manufactured Institute of Geotechnics at the Slovak Academy of Sciences in Košice (ÚGt SAV in Košice). The horizontal drilling stand is designed for rotary rock drilling with small-diameter diamond drill bits up to a diameter of 80 mm. The device enables the drilling of rock samples in the shape of a block with dimensions of  $a \times b \times c$  up to the size of  $300 \times 200 \times 200$  mm. Essential parts of the drilling device are three main units, namely a direct current (DC) motor, a hydro-generator, and a water pump. Their action is the dominant excitation effect resulting in an appropriate vibration response of the entire drilling stand [17–20]. Measurements of acceleration vibrations were designed in the dominant horizontal direction to obtain the vibration response of the drilling rig. Measurements were carried out at the set operating modes, i.e., if only one of the three aggregates of the facility was in operation (I.–III.), if there was always a pair of aggregates in operation (IV.–VI.), and if all three aggregates were in operation (VII.–IX.). The following operating modes have been proposed for industrial practice and experimental research:

- I. motor only;
- II. pump only;
- III. hydro-generator only;
- IV. motor and pump;
- V. motor and hydro-generator;
- VI. pump and hydro-generator;
- VII. motor, pump, and hydro-generator, tool spindle without the bit;
- VIII. motor, pump, and hydro-generator, tool spindle with the bit;
- IX. andesite rock drilling.

The conceptual scheme of experimental methodology and processing of the vibro-acoustic signal is shown in Figure 1.

The vibration response of the drilling rig and its main aggregates is a random process [21–24]. For this reason, it is necessary to base the analysis and rely on signal processing

methods in the time and frequency domain [25–27]. In this case, the vibration response of the drilling device is the acceleration of the vibration motion. Figure 2 shows an overall view of a horizontal drilling stand located in a laboratory.

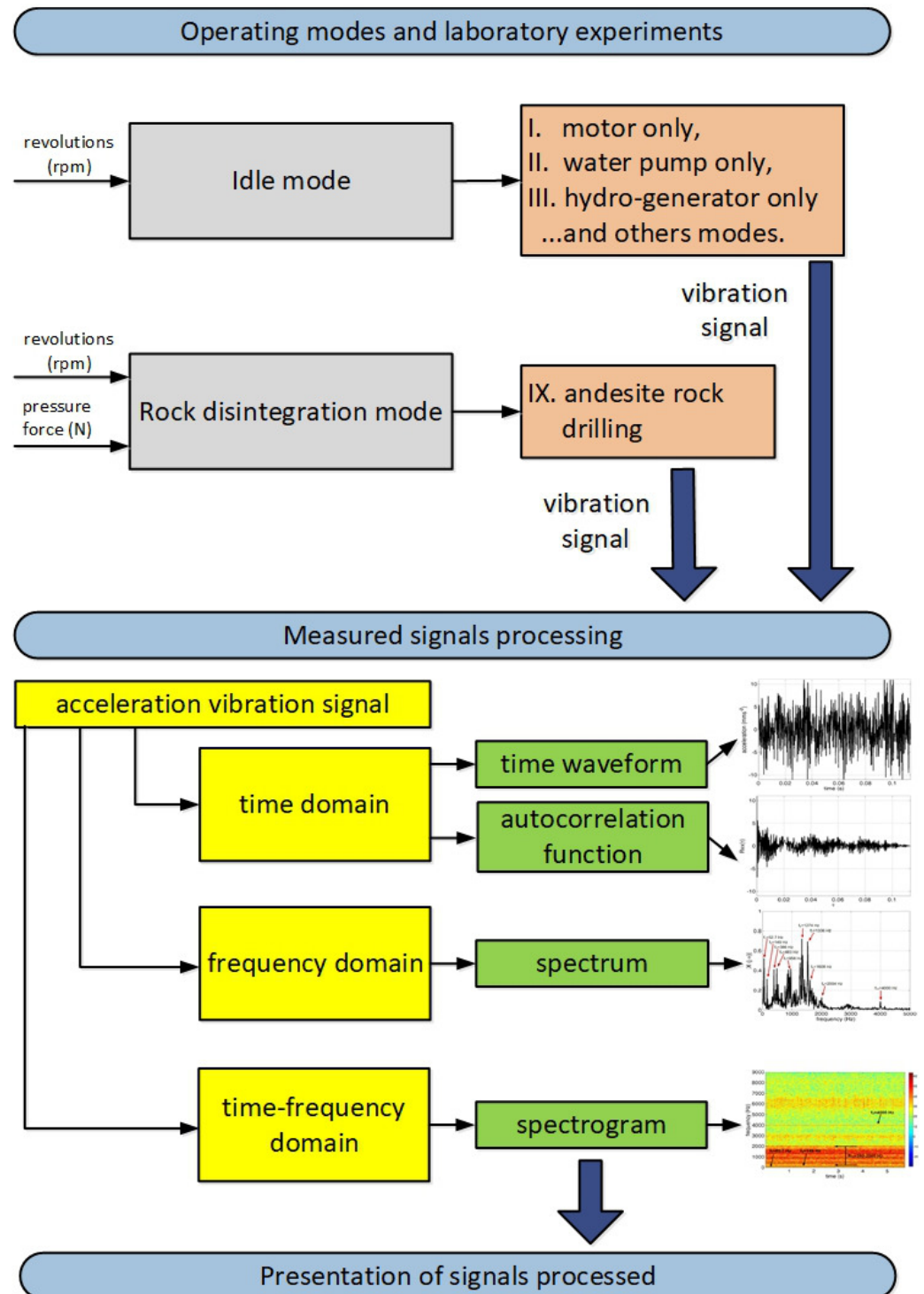
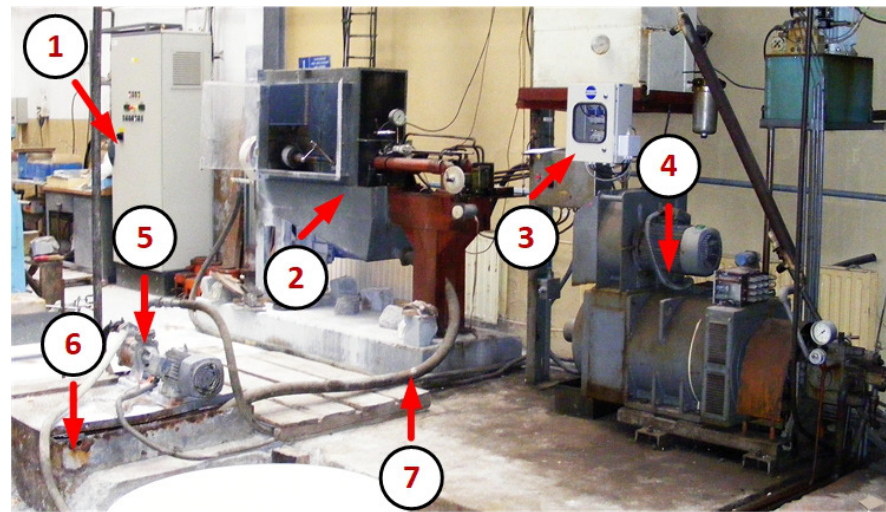


Figure 1. Experiments methodology.



**Figure 2.** Main parts of the drilling stand (1—Power switchboard, 2—experimentally drilling machine, 3—measuring system ADASH, 4—hydroelectric generator, 5—water pump, 6—sludge pit, 7—hose for outfall of drilling fluid).

The horizontal drilling device consists of a support stand (9), on which a headstock with a drilling spindle core (5) is mounted, and a working tool of a standard size drill bit is screwed on. The drilling spindle is driven by a DC motor (12.5 kW, 220 V) via V-belts (3) in a sheet metal housing. The direct current source for the electric motor's drive is a thyristor rectifier. The rinsing liquid water is supplied from the water pump by a rubber pressure hose (1) connected via a sealing head (2) to the drilling spindle. The rock sample (6) is clamped in a mechanical jig (7) which is mechanically connected to a strain gauge head of axial pressure and torque. Parts of the device from the headstock through the core (5) to the clamping device (7) are located in a protective sheet metal housing (4). The strain gauge head is articulated to the piston rods of the hydraulic cylinders. The slider guide is firmly connected to the stand (9). The rinsing liquid is drained from the sedimentation tank (8) via a high-pressure hose (see Figure 2).

The following figures (see Figure 3) describe and present essential parts of the drilling rig in more detail.

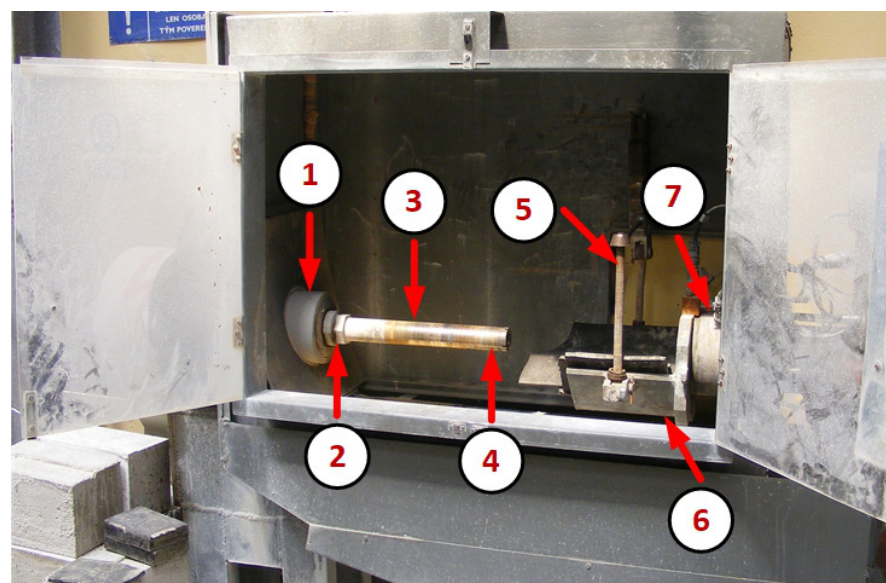


**Figure 3.** Detailed view to the drilling rig (1—headstock, 2—spindle drill, 3—core barrel, 4—drilling bit, 5—clamping mechanism, 6—centering sled clamping mechanism, 7—head of the tensimeter sensor).

Adjustable working parameters of the horizontal drilling stand are the following:

- pressure force,  $F$  0—16,000 N;
- revolutions,  $n$  0–2500 rpm, or 0–50 rps;
- torque,  $M_k$  0–200 Nm;
- drilled length,  $l$  0–0.3 m;
- volume flow of water flush,  $Q$   $0-1 \times 10^{-3} \text{ m}^3\text{s}^{-1}$ ;
- speed (velocity) of drilling,  $v$   $0-16.8 \times 10^{-3} \text{ ms}^{-1}$ .

Even in laboratory conditions, practical drilling results are the rock drilling core (see Figure 4).

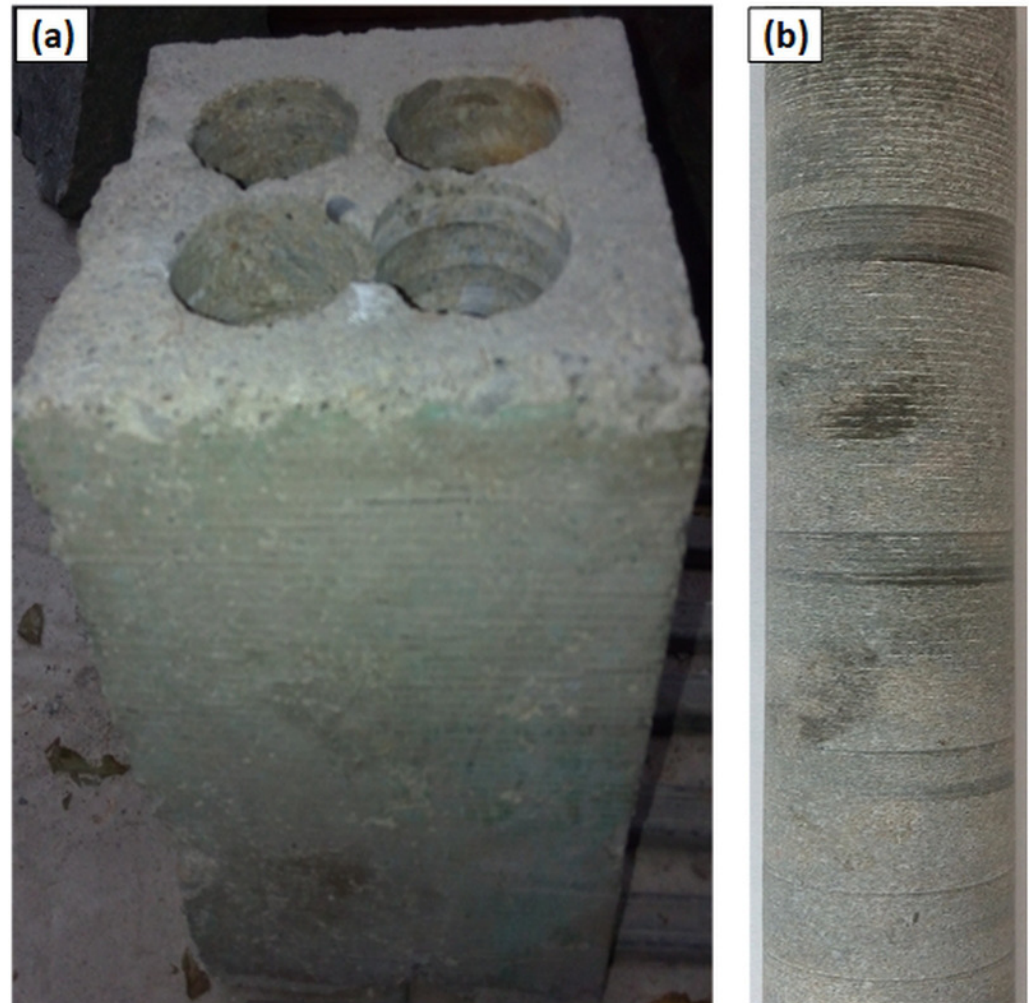


**Figure 4.** Result of practical drilling in laboratory conditions ((a) block-shaped rock sample with boreholes, (b) drilling rock core).

### 3. Theoretical Background and Calculation

#### 3.1. Time Domain Vibration Analysis

Values of oscillating motion parameters the vibration signal respectively generally changes over time [28–30]. For evaluation purposes, it is usually necessary to have a peak, peak-to-peak, and the total energy content of the signal, which is given by the average and effective value [31,32].

The following are considered essential time characteristics for the vibration acceleration signal:

- amplitude  $x(t)$ , which is the instantaneous value of the monitored signal parameter in time  $t$ ;

- peak  $x_p(t)$ , that represents the maximum distance of the peak of the wave from the reference value, usually the  $x$ -axis;
- peak-to-peak  $x_{pp}(t)$ , which is the maximum distance of opposite peaks of the wave;
- the average value  $x_{avg}(t)$  that represents the average value of the amplitude during the wave according to the equation:

$$x_{avg}(t) = \frac{1}{N} \sum_{i=1}^N |x_i(t)|; \quad (1)$$

- effective value (Root Mean Square—RMS) which is the objective value used in the diagnostic guidelines, determined by the equation [33]:

$$\text{RMS} = \sqrt{\frac{1}{N} \sum_{i=1}^N x_i^2(t)}. \quad (2)$$

The established statistical characteristics evaluate the vibration signal only statically at a given time and do not provide information about the dynamic properties of the signal [34–37]. They do not contain information on the statistical dependence of the signal realization values at two different time points  $t_1$  and  $t_2$ .

The dynamic properties of changes over time are characterized by an autocorrelation function in evaluating a single signal. The autocorrelation function can be evaluated from a single implementation of the measured signal and the mutual time shift  $\tau = t_2 - t_1$ . Although, in general, the autocorrelation function depends on the time points  $t_1, t_2$  resp.  $t_2 - t_1$ , in the case of a stationary signal, it depends only on  $\tau$ .

An essential statistical characteristic in time analysis is the signal's autocorrelation, resp. autocorrelation function  $R_{xx}(\tau)$  of the measured vibration signal  $x(t)$ . The autocorrelation function  $R_{xx}(\tau)$  is determined from one implementation and represents a generalization of the mean value of the product of time-shifted values. The following equation defines it:

$$R_{xx}(\tau) = \frac{1}{N} \sum_{i=1}^N x_i(t)(t + \tau). \quad (3)$$

The periodic parts of the vibrational signal  $x(t)$  remain in the autocorrelation function, and the non-periodic ones quickly disappear. From the autocorrelation function, it can be determined the period of the periodic part of the measured signal. The autocorrelation function provides an information about the dependence of the values of the function  $x(t)$  at time  $t$  from the values at time  $t + \tau$ .

From the time waveform of the autocorrelation function, it can be said for practice that the faster the autocorrelation function decreases for increasing  $|\tau|$  [38], the smaller the statistical dependence of the signal's successive values  $x(t)$  and the signal will also cover a broader frequency spectrum. The slower time waveform of the autocorrelation function is characterized by more significant statistical dependencies of successive signal values and greater system inertia. If the signal contains a periodic component, the autocorrelation function has the same period as the signal.

### 3.2. Frequency Domain Vibration Analysis

Frequency domain signal processing, when used correctly, eliminates the shortcomings of a time-domain analysis [39,40]. The method makes it possible to locate emerging faults vibrations of individual parts of the monitored drilling machine [41–43]. The amplitude spectrum of the measured vibration signal  $x(t)$  is obtained by frequency analysis.

The basis of frequency analysis is mainly Discrete Fourier Transform (DFT) and Fast Fourier Transform (FFT). The measured time-varying vibration signal is then processed numerically [44]. The vibration acceleration signal  $x(t)$  is sampled in the time-domain in the analog-to-digital converter (ADC).

Its values are determined at time points distant by the regular sampling period  $T_s$  (i.e., sample time) at the sampling frequency  $f_s$ . Because in practice, only a finite number,  $N$ , of measured signal samples is available, it is necessary to use a discrete Fourier transform.

Before signal processing by the DFT method or FFT algorithm is necessary to be aware of the basic parameters in the calculations:

- frequency range represents the baseband from 0 Hz to  $f_s/2$ ;
- “zoom” factor, when using a frequency magnifier, indicates how many times the frequency range is smaller;
- the number of spectral lines is usually  $N/2$ ;
- the sequence number of the spectral line;
- frequency analysis resolution, indicating the spacing between the spectral lines.

The used Fourier transform  $X(j\omega)$  to obtain the amplitude spectrum of the vibration signal  $x(t)$  from individual parts of the monitored drilling rig is defined by the integral equation:

$$X(j\omega) = \int_{-\infty}^{\infty} x(t)e^{-j2\pi ft} dt. \quad (4)$$

If a directly measured signal generated by any part of the drilling rig is processed, a numerical method known as Discrete Fourier Transform (DFT) is used [45]. It is suitable for calculation (DFT) to use an efficient Fast Fourier Transform (FFT) algorithm, which is used to process vibration signals in the frequency domain to obtain the resulting amplitude spectrum. The following equation defines DFT:

$$X(k) = \sum_{n=0}^{N-1} x(n)e^{-j2\pi k \frac{n}{N}}, \quad n = 0, \dots, N-1; \quad k = 0, \dots, N-1. \quad (5)$$

The discrete value  $X(k)$  represents the amplitude. The values of  $x(n)$  and  $X(k)$  have the same physical dimension.

In industrial practice, power spectra are also calculated in addition to amplitude spectra [46,47]. In some complex industrial processes, in which signals are generated, they have a stronger informative value about the current state of the technological process [48,49]. The following equation was used to calculate the power spectrum:

$$S_{xx}(\omega) = \frac{1}{2\pi N} \left| \sum_{n=1}^N x(n)e^{-j2\pi f_n} \right|^2, \quad (6)$$

where  $1 \leq n \leq N$  applies to a signal in the discrete form  $x(n) = x(n\Delta t)$  with a finite number of samples  $N$ .

The amplitude and power spectra of vibration signals from individual parts of the monitored drilling rig were analyzed. The FFT algorithm was used for the measured signal with a sampling frequency of  $f_s = 18$  kHz to obtain a range from 0 to 9 kHz, a sampling period of  $T_s = 0.55 \mu s$  a segment length of  $N = 2048$  samples. The measured sampled signal was used; therefore, mathematical equations in a discrete form are presented.

### 3.3. Time-Frequency Domain Vibration Analysis

When processing signals whose nature changes rapidly over time, it is often useful to consider the frequency content of the short signal segments. It makes it possible to formulate a more general spectrum as a two-dimensional function, dependent not only on frequency but also on time position. The time-frequency analysis is practically based only on the finite signal segments. Classical frequency analysis is about determining the harmonic components of different frequencies [50–52]. However, in time-frequency analysis, it is a matter of the most accurate localization of the occurrence of the signal's frequency components, both frequency, and time data. The spectrogram as a basis of time-frequency analysis is one of the important tools of technical diagnostics. The spectrogram

expresses changes in the power spectrum of the signal over time. In the case of evaluating a vibration signal, time-frequency analysis can be useful in examining changes in the spectral properties of the signal due to a change in the properties of the object being monitored. The graphical representation of the spectrogram is in the form of image information. It can be understood as a highly integrative source of information. Its information value is high compared to simpler forms of information. The spectrogram of random vibration signal is a sequence of spectra calculated one after the other. Thus, a spectrogram can be expressed as a time sequence of its power spectra, where these power spectra have the structure of  $N/2$  element vectors (7).

$$S_{xx}(f_k, j) = [S_{xx}(f_0, j), S_{xx}(f_1, j), \dots, S_{xx}(f_{\frac{N}{2}-1}, j)]. \quad (7)$$

The elements  $S_{xx}(f_k, j)$  of the power spectrum are the file mean values associated with the  $j$ -th time moment and the  $k$ -th power frequency component of the signal  $f_k$ . Parameter  $N$  represents the number of samples in the segment of this signal.

#### 4. Experimental Results and Analysis

The operation of the horizontal drilling stand in idle modes and during the rock drilling process generates a vibration signal. It is evident that the vibration signal generated by the technological drilling equipment carries up-to-date information characterizing its technical condition and drilling process [53,54].

The presented experimental modes of operation of the device, measurement, processing, and analysis of vibration acceleration signals identify and classify significant vibration sources in the drilling process. Their identification is essential in industrial practice in terms of wear of drill stand and drill bit parts [55,56], reducing the cost of the drilling process, increasing drilling efficiency, reducing vibrations, and their impact on the working environment and humans.

Stand idle modes with individual aggregates without drill bit and rock drilling can represent reference modes to other set experimental modes.

##### 4.1. Vibration Signal Processing in the Time Domain

The basic processing of vibration signals of acceleration in the time domain from the drilling stand aggregates was the display of time waveforms, auto-correlation functions, and the calculation of essential statistical characteristics.

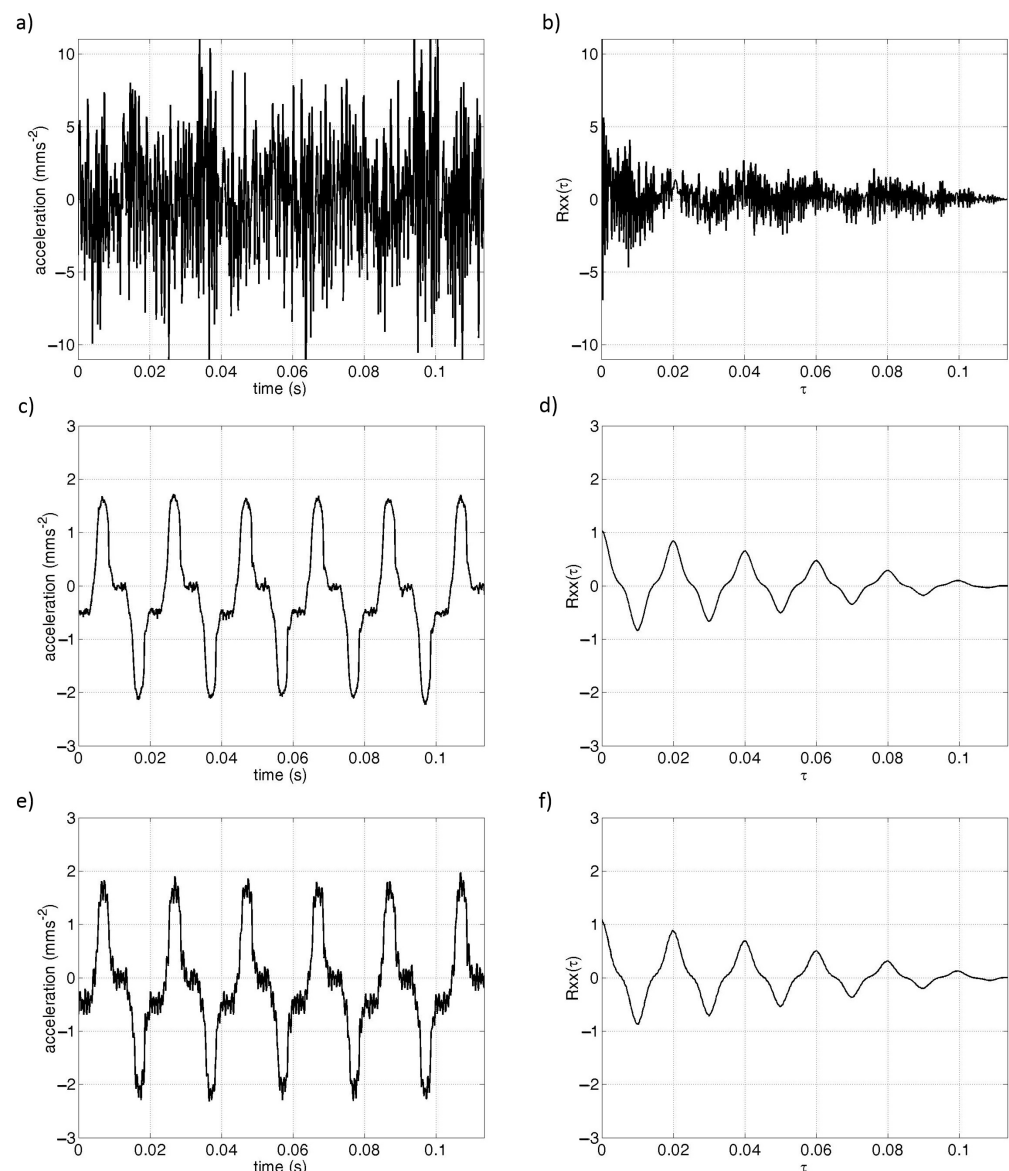
In the time domain, the amplitudes  $x(t)$ , peak  $x_p(t)$ , peak to peak  $x_{pp}(t)$ , average  $x_{avg}(t)$ , and RMS of the vibration signal from individual modes were observed. For idle modes I. to VIII. the stand revolutions were set at 1000 (rpm) or 16.67 (rps) without pressure force, as there was no direct disintegration of the rock, for mode IX., the revolutions were set to 1000 (rpm), and the pressure  $F = 8000$  N.

The measurement of one experimental mode took  $t = 6$  s at a sampling frequency of  $f_s = 18,000$  Hz and a sampling period of  $T_s = 55.5$   $\mu$ s. All regime measurements were performed by an analogous principle. A segment with the number of samples  $N = 2048$  was processed from the entire measured signal.

Figures 5–7 show the time waveforms and associated auto-correlation functions of the vibration acceleration signals for the set operating modes of the drilling rig. The acceleration signals' time waveforms and auto-correlation functions at the number of samples  $N = 2048$  are more readable. A more detailed display is chosen for a more straightforward idea of the time waveform of the measured signal. It is possible to deduce the essential statistical characteristics from the time waveforms directly.

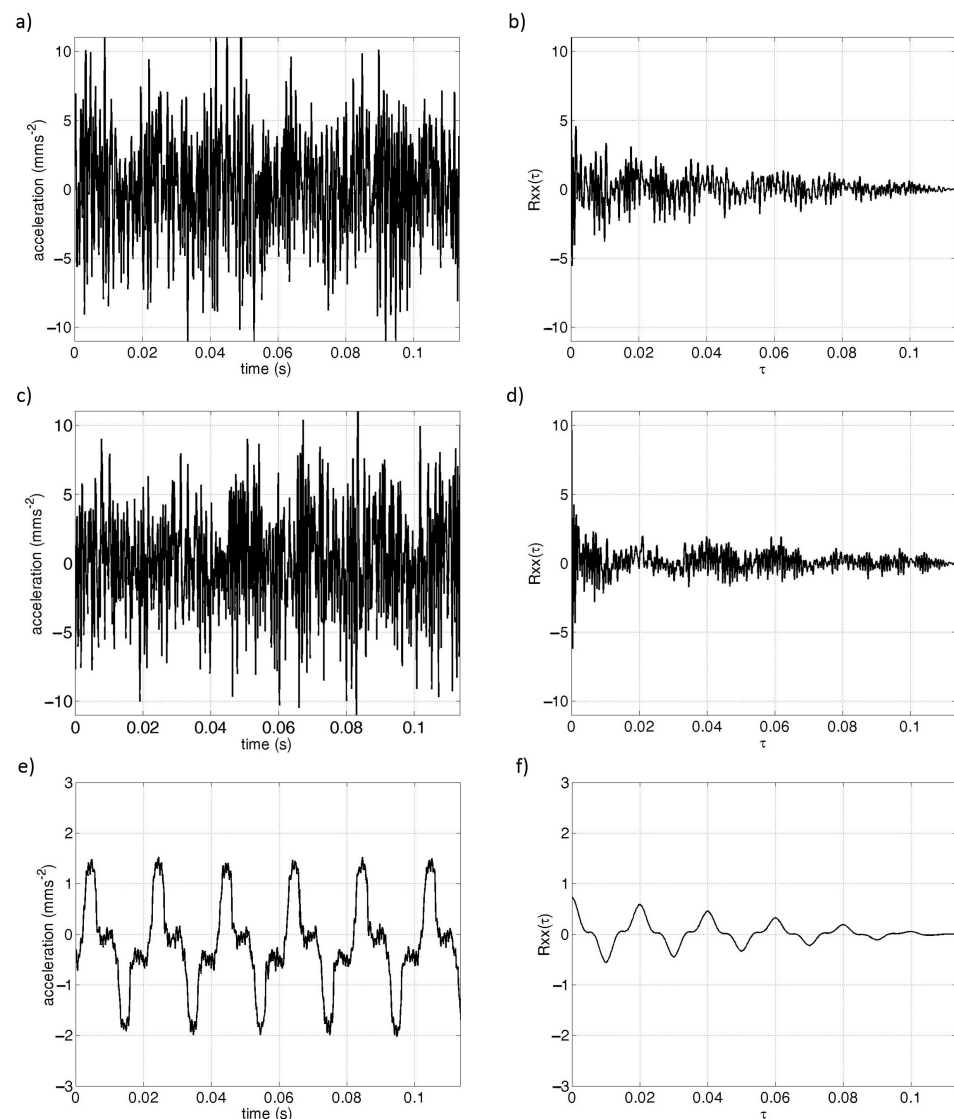
Figure 5 shows the time waveforms of the separately measured signals of the motor, pump, and hydro-generator units, representing the operating modes I.–III. If modes I.–III. are compared, then the highest values of significant statistical characteristics are at the vibration signal from the motor, i.e.,  $x_p(t) = 12.753$ ,  $x_{pp}(t) = 25.836$ , and  $RMS = 3.831$  (see Table 1). It is clear that the motor aggregate is the main vibration generator (see Figure 5a).

The pump achieves the lowest statistical value. It is clear from the time waveforms that the pump and hydro-generator units have non-harmonic composite periodic signals with a weak stochastic component (see Figure 5c,e). The time waveform of the auto-correlation function also indicates this. In contrast, the waveform of a motor unit is strongly stochastic, but it is assumed to include periodic components even if the random component overlaps a composite signal containing essential diagnostic information. The auto-correlation function of the motor decreases rapidly with increasing  $\tau$ , meaning that the signal values have less statistical dependence (see Figure 5b) and assume a broad frequency spectrum. In contrast, the auto-correlation functions of the pump (see Figure 5d) and the hydro-generator (see Figure 5f) have a gradual descent of the samples, representing a greater statistical dependence and a narrow frequency spectrum.



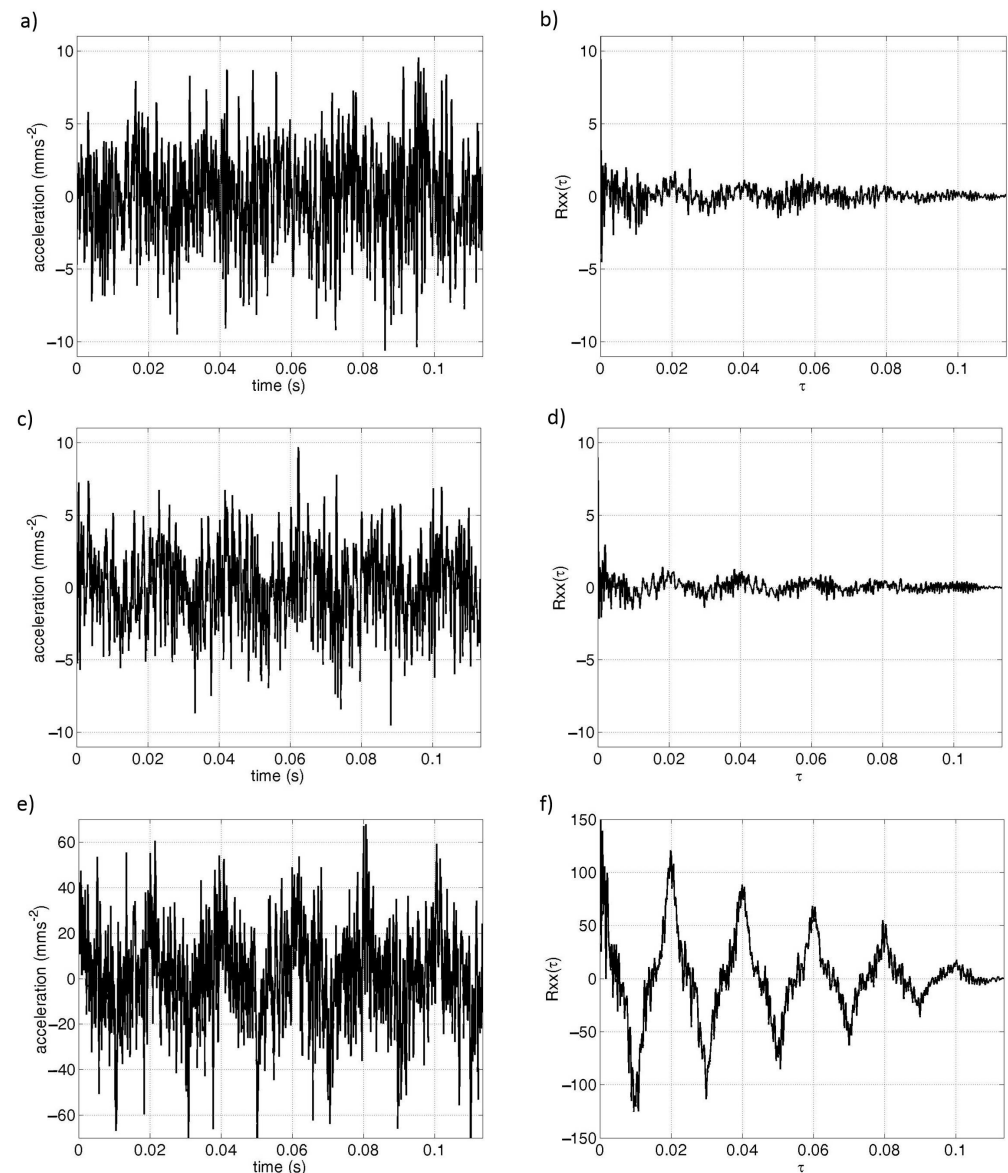
**Figure 5.** Time waveforms of the separately measured signals of the motor, pump, and hydro-generator units ((a) the time waveform of the vibration signal of the motor, (b) the auto-correlation function of the motor, (c) the time waveform of the vibration signal of the pump, (d) the auto-correlation function of the pump, (e) the time waveform of the vibration signal of the hydro-generator, (f) the autocorrelation function of the hydro-generator).

Figure 6 shows the time waveforms of the measured signals during the operation of the pair of aggregates in the operating modes IV.–VI. The combinations are motor and pump, motor and hydro-generator, pump and hydro-generator. If the modes IV.–VI. are compared with each other, then the highest values of statistical characteristics are again at the vibration signals where the motor, i.e., motor and pump, motor and hydro-generator, modes IV. enter into the measurement, modes IV. and V. (see Table 1). The position of the motor unit as the primary source of vibration is confirmed. The lowest statistical values are reached by mode VI., i.e., pump and hydro-generator  $x_p(t) = 1.542$ ,  $x_{pp}(t) = 3.622$ ,  $RMS = 0.904$ . It is clear from the time waveforms that the units in mode VI., i.e., the pump and the hydro-generator, are non-harmonic periodic signals, quasi-periodic with a stochastic component (see Figure 6e). It confirms the time waveform of the auto-correlation function (see Figure 6f). On the contrary, the signal waveforms of modes IV. and V. are strongly stochastic. The strong source of acceleration vibration is the motor unit. Regimes IV. and V. were successful. In a broader context, they have similar auto-correlation (see Figure 6b,d) and time waveforms (see Figure 6a,c).



**Figure 6.** Time waveforms of the measured signals during the operation of the pair of aggregates in the operating modes IV.–VI. ((a) motor and pump vibration signal time waveform, (b) motor and pump auto-correlation function, (c) motor and hydro-generator vibration signal time waveform, (d) motor and hydro-generator vibration auto-correlation function, (e) pump and hydro-generator vibration signal time waveform, (f) autocorrelation function of pump and hydro-generator).

Operating modes VII.–IX. compared to other regimes (see Figure 7), i.e., I.–VI., have significantly higher values of statistical characteristics (see Table 1). The reason is that all three aggregates are active during operating modes. In working mode VIII. a drill bit was installed on the spindle as part of the research and subsequent evaluation of the vibration signal (see Figure 7c,d). The proposed working mode VII. is without a drill bit on the spindle (see Figure 7a,b).



**Figure 7.** Time waveforms of the measured signals during the operation of the pair of aggregates in the operating modes VII.–IX. ((a) time waveform of the signal of three aggregates without a drill bit, (b) auto-correlation function of three aggregates without a drill bit, (c) time waveform of the signal of three aggregates with a drill bit, (d) auto-correlation function of three aggregates with a drill bit, (e) time waveform of the andesite rock disintegrating signal, (f) auto-correlation function of the andesite rock disintegrating signal).

In the last investigated regime IX., is a direct interaction of the drill bit with the andesite rock to disintegrate it (see Figure 7e,f). The revolutions and pressure force mode parameters were set to  $n = 1000$  rpm and  $F = 8000$  N. For this mode, the observed values of the vibration signal are clearly the highest, i.e.,  $x_p(t) = 76.205$ ,  $x_{pp}(t) = 160.711$ , and  $RMS = 21.978$ . The time waveforms of the signals are stochastic and stationary. It is clear

from the time waveform of the autocorrelation function that the investigated processed signal also has periodic components.

Figure 8a shows a histogram with a normal Gaussian distribution. It characterizes the operating modes in which the main vibration generator is the motor (i.e., modes I., IV., V., and VII.–IX.). For modes without motor operation (i.e., II., III., and VI.). The characteristic histogram in the figure is Figure 8b. It can be classified as a two-vertex histogram or a histogram with a non-Gaussian distribution. It indicates a superposition and a significant change in the position of the measured signals [57,58].

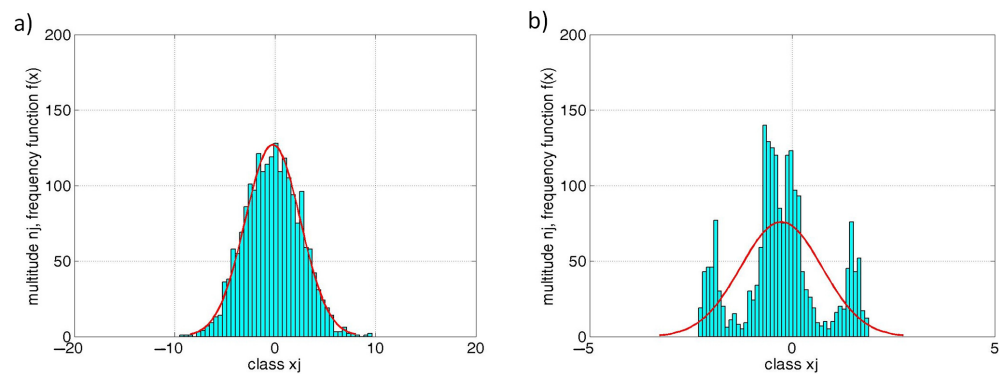


**Figure 8.** Histogram of probability distribution of measured signals ((a) normal Gaussian distribution, (b) non-Gaussian distribution).

**Table 1.** Statistical characteristics of operating modes.

Operating Mode	Peak	Peak-to-Peak	Average Value	RMS
1. motor	12.753	25.836	−0.276	3.831
2. water pump	1.646	3.787	−0.261	0.979
3. hydro-generator	1.931	4.326	−0.249	1.032
4. motor and water pump	13.2325	26.016	−0.232	3.697
5. motor and hydro-generator	12.065	26.657	−0.267	3.576
6. water pump and hydro-generator	1.542	3.622	−0.245	0.904
7. motor, water pump and hydro-generator, tool spindle without the bit	13.247	27.752	−0.2767	3.552
8. motor, water pump and hydro-generator, tool spindle with the bit	9.939	20.343	−0.292	2.948
9. andesite drilling	71.1702	159.4525	0.14856	21.1312

In the working modes I.–IV.–V. and VII.–VIII.–IX., the measured vibration signal of motor acceleration have higher statistics parameters; the highest contains IX. mode. When the drill bit was placed on the spindle, the values decreased. It suggests that the drill bit has a partially stabilizing character on the drilling stand.

The complex classification of processed vibration signals in the time domain is complex. Acceleration vibration signals in operating modes I.–IV.–V. and VII.–VIII.–IX. are stochastic and stationary but have overlapping periodic and quasi-periodic components. The least significant statistical component appears to be the mean value of the signals. The individual values of the modes do not differ significantly.

Measured and processed vibration signals from the pump and hydro-generator, i.e., modes II.–III.–VI. are classified as non-harmonic, compound periodic, or quasi-periodic with the weak stochastic component.

The fact that there are periodic components in individual signals will be proved by processing and evaluation in the frequency and time-frequency domain.

The processing of the measured vibration acceleration signals by time analysis assumes that the generated vibration emissions are a possible reference source of information about the current state of the observed aggregates and the disintegration process.

The vibration signal is an indicator of faultless operation of the units and a vibration generator in the working environment.

Obviously, the time characteristics are not entirely sufficient to analyze the properties of the vibration signal at steady-state modes. However, in the case of dynamic changes in the drilling mode, such as a change in revolutions, pressure force, disintegrating tool, or a change in the type of disintegrating rock, monitoring the ongoing changes in the frequency domain is effective.

#### 4.2. Vibration Signal Processing in the Frequency Domain

The processing of vibration acceleration signals from individual aggregates in the frequency domain requires the construction of amplitude and power spectra. It is possible to differentiate dominant frequencies, frequency clusters, and frequency bands from the spectra. An algorithm of FFT constructed the resulting operating mode frequency spectra.

The algorithm of FFT was used for a vibration signal with a sampling frequency of  $f_s = 18$  kHz, a sampling period of  $T_s = 55.5$   $\mu$ s, and a segment length of  $N = 2048$  samples. Frequency spacing must be considered when analyzing and constructing signal spectra. The frequency spacing between the spectral lines indicates the density of the spectral lines. Denser spectral lines increase the frequency resolution of the constructed spectra. The frequency spacing in the spectra was determined by the following equation:

$$\Delta f = \frac{f_s}{N} = \frac{18000 \text{ Hz}}{2048} = 8.7 \text{ Hz.} \quad (8)$$

Significant dominant frequencies and frequency bands are recognizable from the amplitude spectra of individual operating modes. Dominant frequencies have a significant amplitude.

The following figures (see Figures 9 and 10) present the resulting amplitude spectra for the operating modes I.–IX. when the individual units are running idle and with a load.

A more detailed display of the constructed spectra (i.e., zoom factor) is chosen for easier and clearer identification and differentiation of dominant frequencies and frequency bands.

From the amplitude–frequency spectrum for mode I. if only the motor unit were in operation, it is clear that the dominant frequency components are in the frequency band 0–4000 Hz. Several clusters have significant frequency components in this frequency band (see Figure 9a). Table 2 lists the significant frequency components. In the frequency spectrum of the motor, it was possible to determine approximately ten dominant frequencies that are characteristic of this aggregate. The spectrum can be said to be broad-spectrum because it contains the basic low frequencies  $f_1 = 52.7$  Hz,  $f_2 = 149$  Hz,  $f_3 = 386$  Hz, and  $f_4 = 483$  Hz. In the mid-frequency band from 1 kHz, there are several significant frequencies  $f_6 = 1274$  Hz and  $f_7 = 1336$  Hz with high amplitude. The spectrum also contains a high frequency  $f_{10} = 4000$  Hz.

From amplitude–frequency spectra for operating mode II., i.e., only the pump is running, and mode III. when in operation is the hydro-generator unit, it is clear that significant frequency components are located in the low-frequency band 0–1000 Hz with one frequency above 1 kHz at the hydro-generator  $f_8 = 1318$  Hz. Operating mode spectrum II. has five dominant frequencies that are characteristic of the aggregate. The fundamental frequencies are  $f_1 = 52.7$  Hz,  $f_2 = 149$  Hz, and  $f_3 = 246.1$  Hz, the other frequencies are non-integer multiples of the fundamental revolutions frequencies (see Figure 9b).

Operating mode spectrum III. has 5 to 7 dominant frequencies in detailed view. It contains the fundamental frequencies and the essential frequencies  $f_7 = 878.9$  Hz and  $f_8 = 1318$  Hz. They represent the significant frequencies that differentiate the pump spectrum from the hydro-generator spectrum. These frequencies are only characteristic of the hydro-generator unit (see Figure 9c).

In operational modes IV. and V., the spectra of 8 to 13 dominant frequencies in a detailed view (see Figure 10d,e) can be observed. Motor vibrations strongly influence the spectra. The frequency band is in the range of 0–4000 Hz. The basic common frequencies are the low frequencies  $f_1 = 52.7$  Hz,  $f_2 = 149$  Hz,  $f_3 = 439$  Hz, and higher 1723 and 4000 Hz. The middle frequency band of both modes is in the range of 1000–3000 Hz. Also in this

band are frequencies with high amplitudes of 1230, 1248, 1362, 1485, and 1529 Hz. This frequency band contains several dominant frequencies closely related to the operation of the motor and pump, motor, and hydro-generator unit combination. The spectrum of these modes was confirmed to be broad-spectrum .

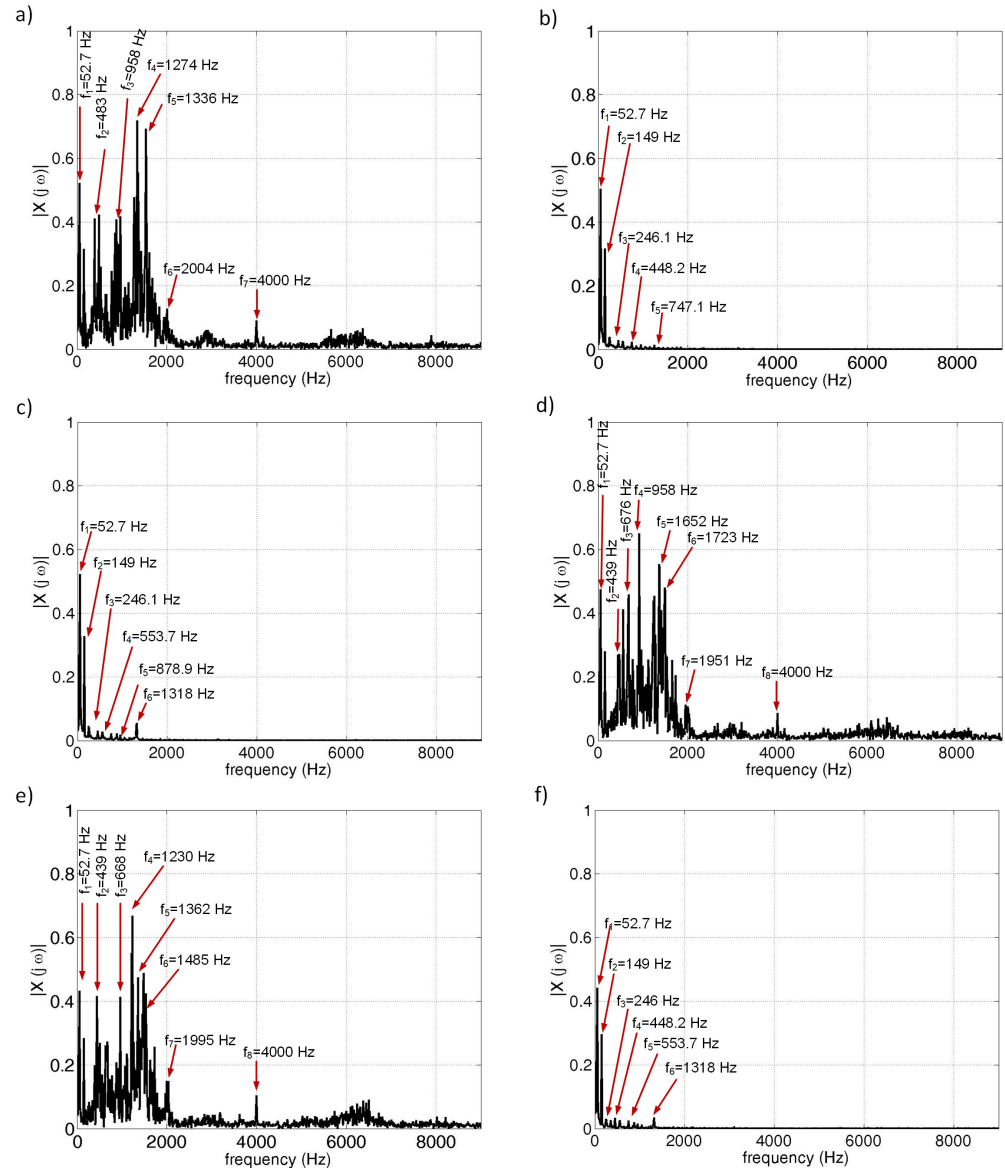


**Figure 9.** Resulting amplitude spectra for the operating modes I–VI. ((a) frequency amplitude spectrum of the motor vibration signal, (b) the pump vibration signal, (c) the hydro-generator vibration signal, (d) the motor and pump vibration signal, (e) the motor and hydro-generator vibration signal, (f) the pump and hydro-generator vibration signal).

The spectrum of the operating mode VI, which represents the operation of the combination of pump and hydro-generator units, is influenced by the strong periodicity of the measured vibration signal. Therefore, it contains the low frequencies of revolutions and its non-integer multiples (see Figure 9f).

From amplitude-frequency spectra for operating modes VII. and VIII., when all three aggregates are in operation, i.e., motor, pump, and hydro-generator, it is clear that significant frequency components are located in the frequency band 0–4000 Hz. In addition, the spectra contain several dominant frequencies and clusters (see Figure 10a,b).

The spectrum of the operating mode IX. (i.e., direct disintegration of the andesite rock), contains besides the frequency band 0–2000 Hz with its dominant frequencies, also a strong

frequency band 6000–9000 Hz. This significant band suggests that this is the part of the spectrum that directly identifies the disintegration of the andesite rock (see Figure 10c).

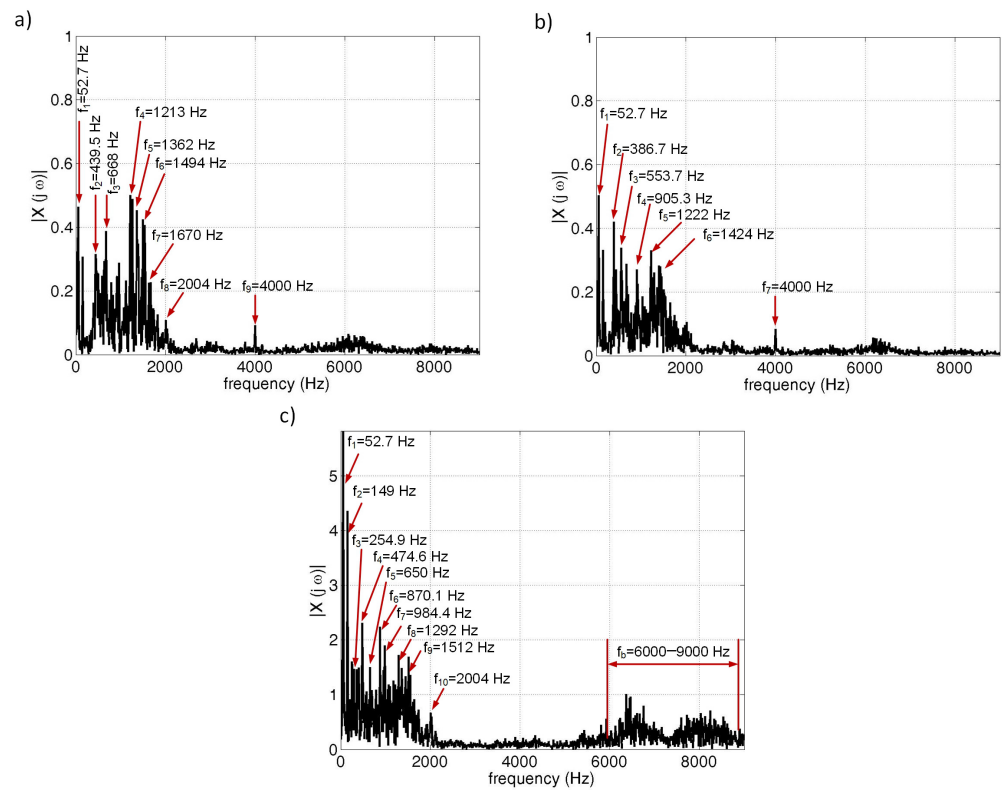


**Figure 10.** Detailed view of dominant frequencies in operational modes VII.–IX. ((a) frequency amplitude spectrum of the vibration signal of three aggregates without drill bit, (b) the vibration signal of three aggregates without drill bit, (c) the andesite rock disintegrating vibration signal).

The presented frequency spectra make it possible to identify and recognize individual dominant frequencies for each mode. Table 2 lists the common and different frequencies. Common frequencies are in the lower frequency band 0–1000 Hz, and differences in the 1000–3000 Hz are visible in the middle frequency band. The most significant differences are in the higher frequency band 4000–9000 Hz. Mainly frequency  $f = 4000$  Hz, which occurs in I., IV. V. VII., VIII. operating modes do not appear in II. III. VI. without the motor. From a scientific and professional point of view, we are most interested in those frequencies that can be directly identified and, at the same time, are different. It is assumed that they characterize the individual aggregates during operation, the andesite rock disintegrating mode, and other random vibrations.

**Table 2.** Dominant frequencies.

Operating Mode	Dominant Frequencies (Hz)											
1. motor	52.73	149	386.7	483.4	958	1274	1336	-	-	1608	2004	4000
2. water pump	52.73	149	246.1	448.2	747.1	-	-	-	-	-	-	-
3. hydro-genertor	52.73	149	246.1	448.2	553.7	747.1	878.9	1318	-	-	-	-
4. motor and water pump	52.73	149.4	439.5	553.7	676.8	958	1248	1529	1652	1723	1951	4000
5. motor and hydro-generator	52.73	149.4	439.5	668	958	1230	1362	1485	1723	1995	4000	-
6. water pump and hydro-generator	52.73	149.4	246	351.6	448.2	553.7	747.1	1318	-	-	-	-
7. motor, water pump and hydro-generator, tool spindle without the bit	52.73	149.4	439.5	668	958	1213	1362	1494	1670	1819	2004	4000
8. motor, water pump and hydro-generator, tool spindle with the bit	52.73	149.4	386.7	553	668	905.3	1222	1424	1644	-	2013	4000
9. andesite drilling	52.73	149.4	254.9	474.6	650	870	984	1292	1512	-	2004	6000–9000

Power spectra are constructed during the analysis of a broad-spectrum vibrational signal with stochastic components in the frequency domain. Frequency amplitude spectra  $|X(j\omega)|$  created by the FFT algorithm are raised to the second power, which gives the

power frequency spectra  $S_{xx}(\omega)$ . By amplifying the amplitudes, the fluctuations in the vibration signal spectrum are reduced. The power spectra constructed by this method are shown in the figures (see Figures 11 and 12).

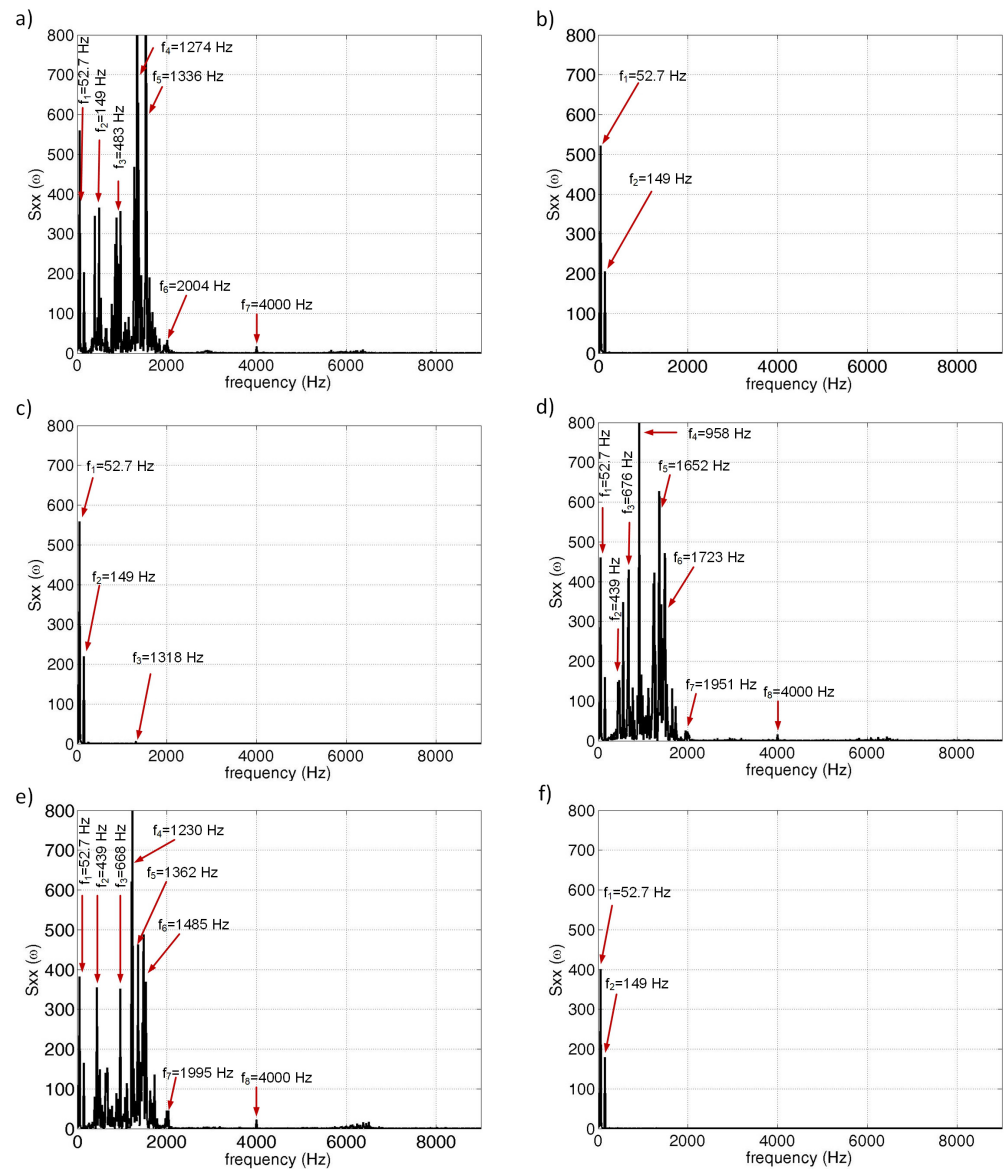


**Figure 11.** Power spectra by FFT algorithm ((a) frequency power spectrum of the vibration signal of the motor, (b) the vibration signal of the pump, (c) the vibration signal of the hydro-generator, (d) frequency power spectrum of vibration signal of motor and pump, (e) frequency power spectrum of vibration signal of motor and hydro-generator, (f) frequency power spectrum of the pump and hydro-generator vibration signal).

If the power spectra are compared with the amplitude spectra in the figures in all modes, it is clear that the dominant frequencies have become visible, and the spectra have been cleared. The number of dominant frequencies has decreased. It is clear that some frequency components of lower power levels have been suppressed, highlighting more power-relevant components.

These frequencies are in the reduced frequency range 0–4000 Hz (see Figure 11a–f and Figure 12a,b). In the IX. mode, the higher frequency band 6000–9000 Hz is of strong importance, which was marked as the band characteristic of andesite rock disintegrating (see Figure 12c).

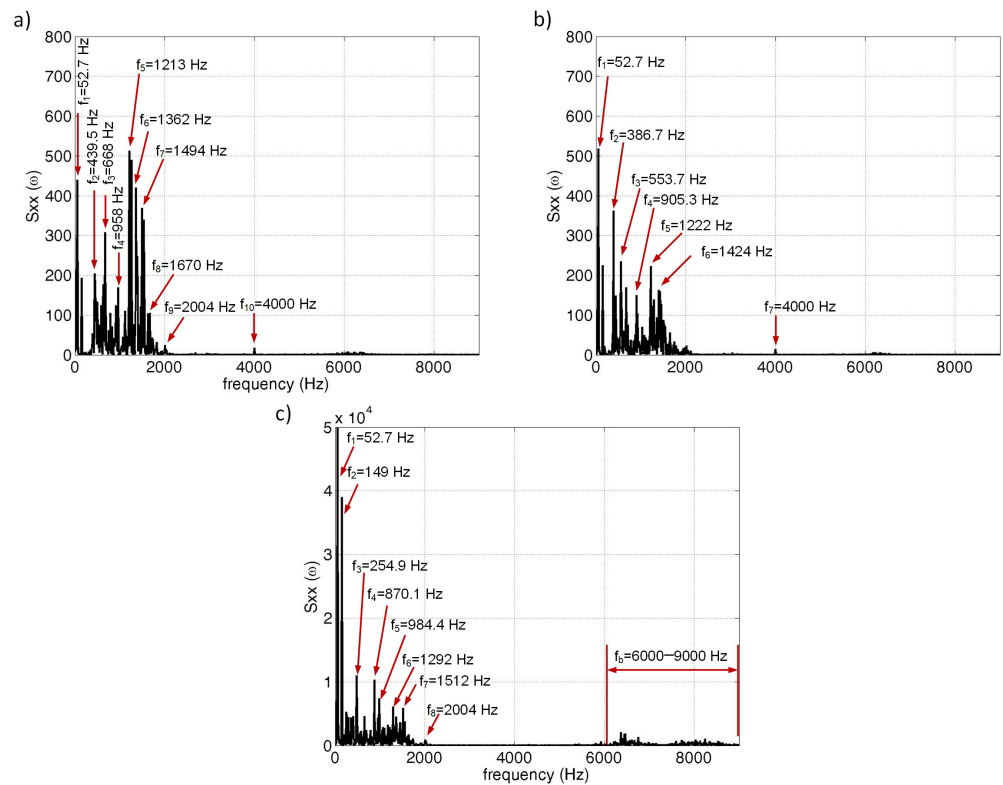


**Figure 12.** Power spectra by FFT algorithm ((a) frequency power spectrum of vibration signal of three aggregates without drill bit, (b) frequency power spectrum of vibration signal of three aggregates with drill bit, (c) frequency power spectrum of the andesite rock disintegrating vibration signal).

#### 4.3. Vibration Signal Processing in the Time-Frequency Domain

The dynamics of the vibration signal of the acceleration of the operating modes and the process of disintegration of the andesite rock can be observed mainly during the construction of the spectrograms.

The spectrograms are the result of time-frequency analysis. It can be stated that they present the presence of frequencies or frequency bands as a function of time. The presented spectrograms are constructed with the time of experimental measurement of the vibration signal  $t = 6$  s at the sampling frequency  $f_s = 18$  kHz and  $T_s = 55.5$   $\mu$ s. The spectrograms were obtained from the operating modes I.–IX. In the figures (see Figures 13–15), the spectrograms are shown in 2D and 3D. Dominant frequencies and frequency bands are marked in 2D and 3D views. Recognition of dominant frequencies from spectrograms is more difficult if they are not individually separated. Such a frequency is  $f = 4000$  Hz. From the spectrograms (see Figure 15e,f), it is clear that the range of the andesite disintegrating frequency is 6000–9000 Hz.

The spectrograms confirm a broad-spectrum vibrational signal, especially when all-important aggregates are in operation and the andesite drilling process.

The processing and presentation of vibrational signals of an acceleration in the frequency domain presented by the spectra and in the time-frequency spectrograms are adequate, consistent, and document the suitability of the algorithms and methods used. Therefore, it can be stated that the analyzes of the measured vibration signals are correct.

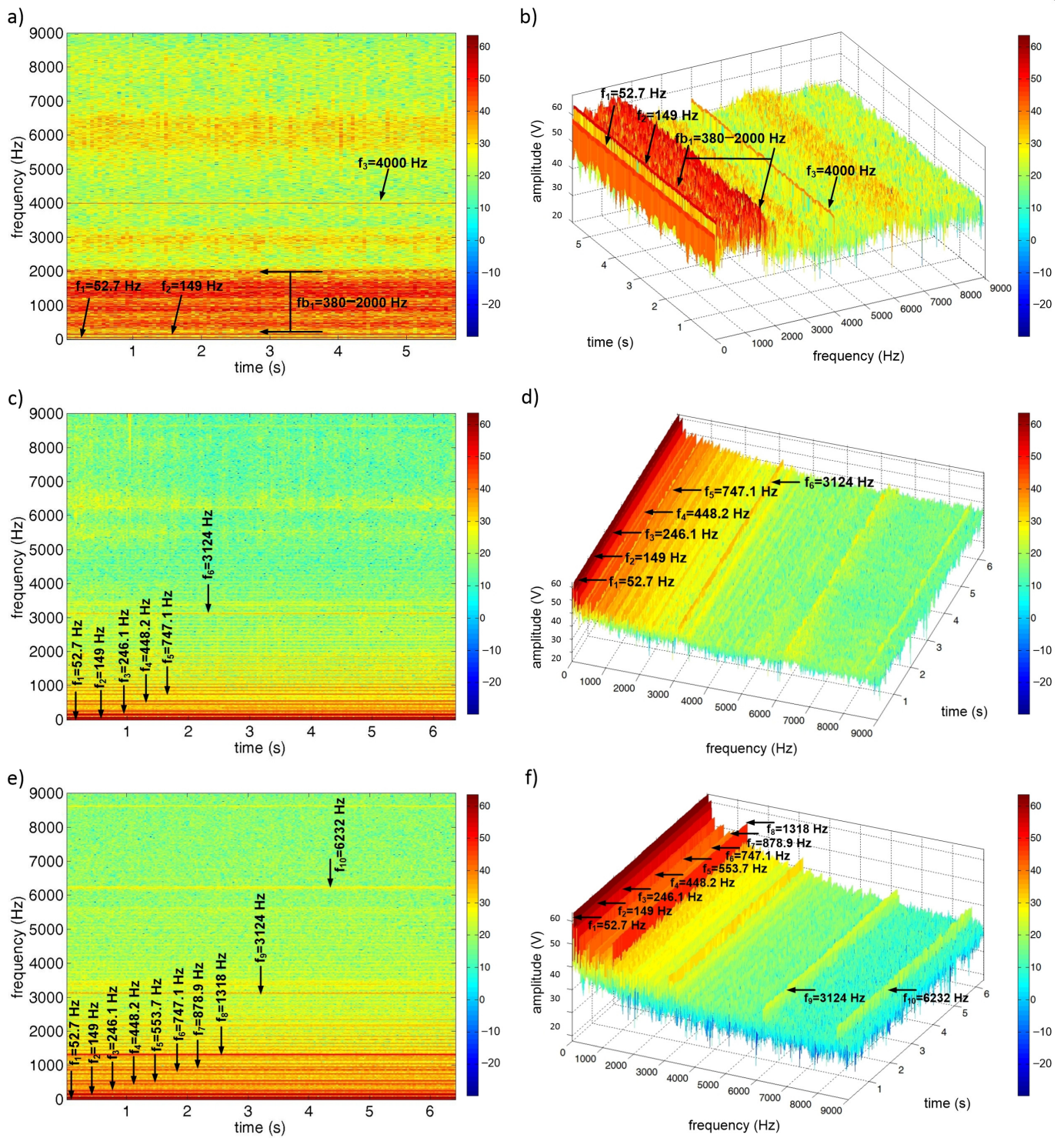


**Figure 13.** Spectrograms of vibration signals of acceleration ((a) 2D view of motor signal spectra, (b) 3D view of motor signal spectra, (c) 2D view of water pump signal spectra, (d) 3D view of water pump signal spectra, (e) 2D view of hydro-generator signal spectra, (f) 3D view of hydro-generator signal spectra).

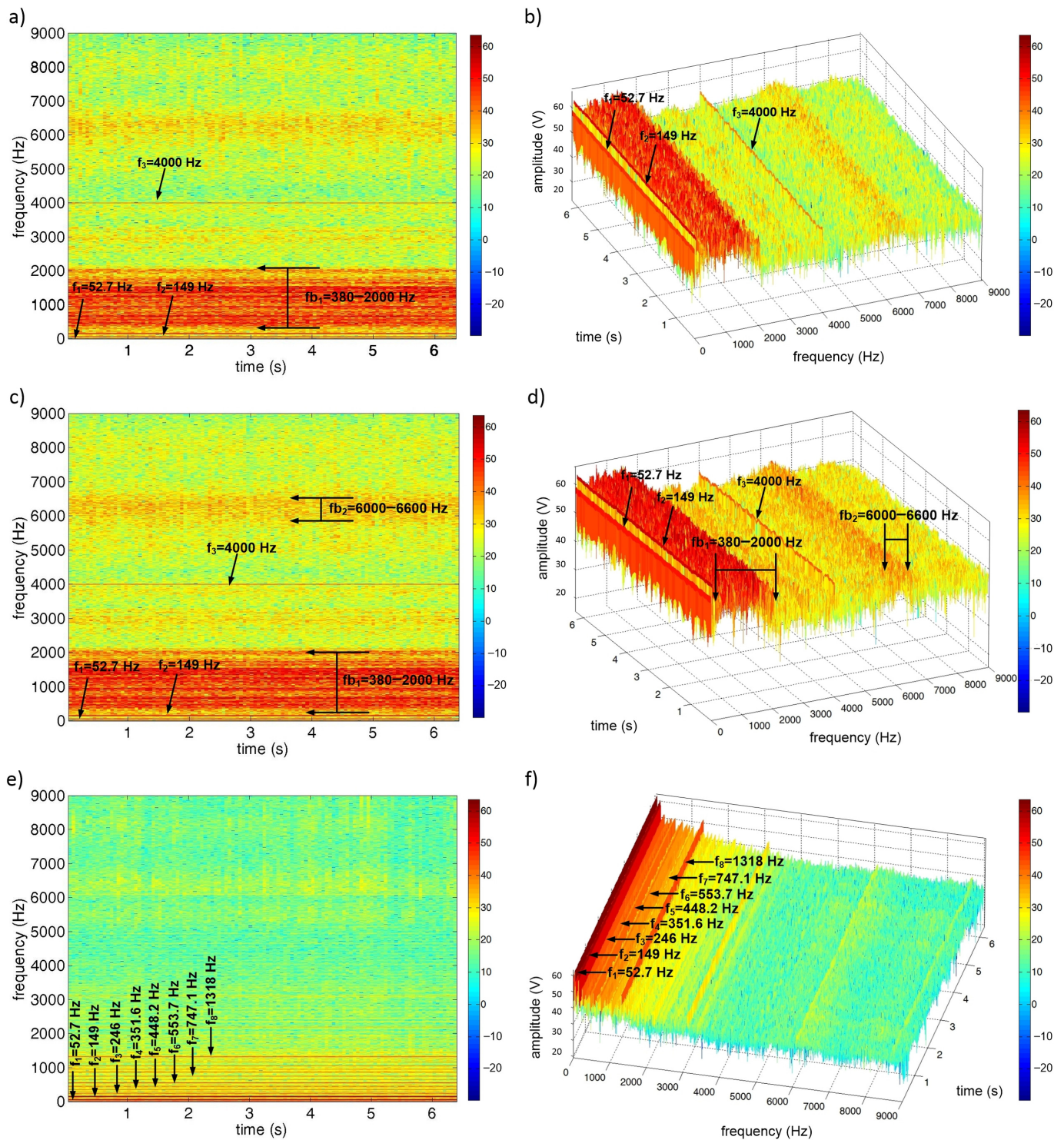


**Figure 14.** Spectrograms of vibration signals of acceleration ((a) motor and pump in 2D view, (b) motor and pump in 3D view, (c) motor and hydro-generator in 2D view, (d) motor and hydro-generator in 3D view, (e) pump and hydro-generator in 2D view, (f) pump and hydro-generator in 3D view).

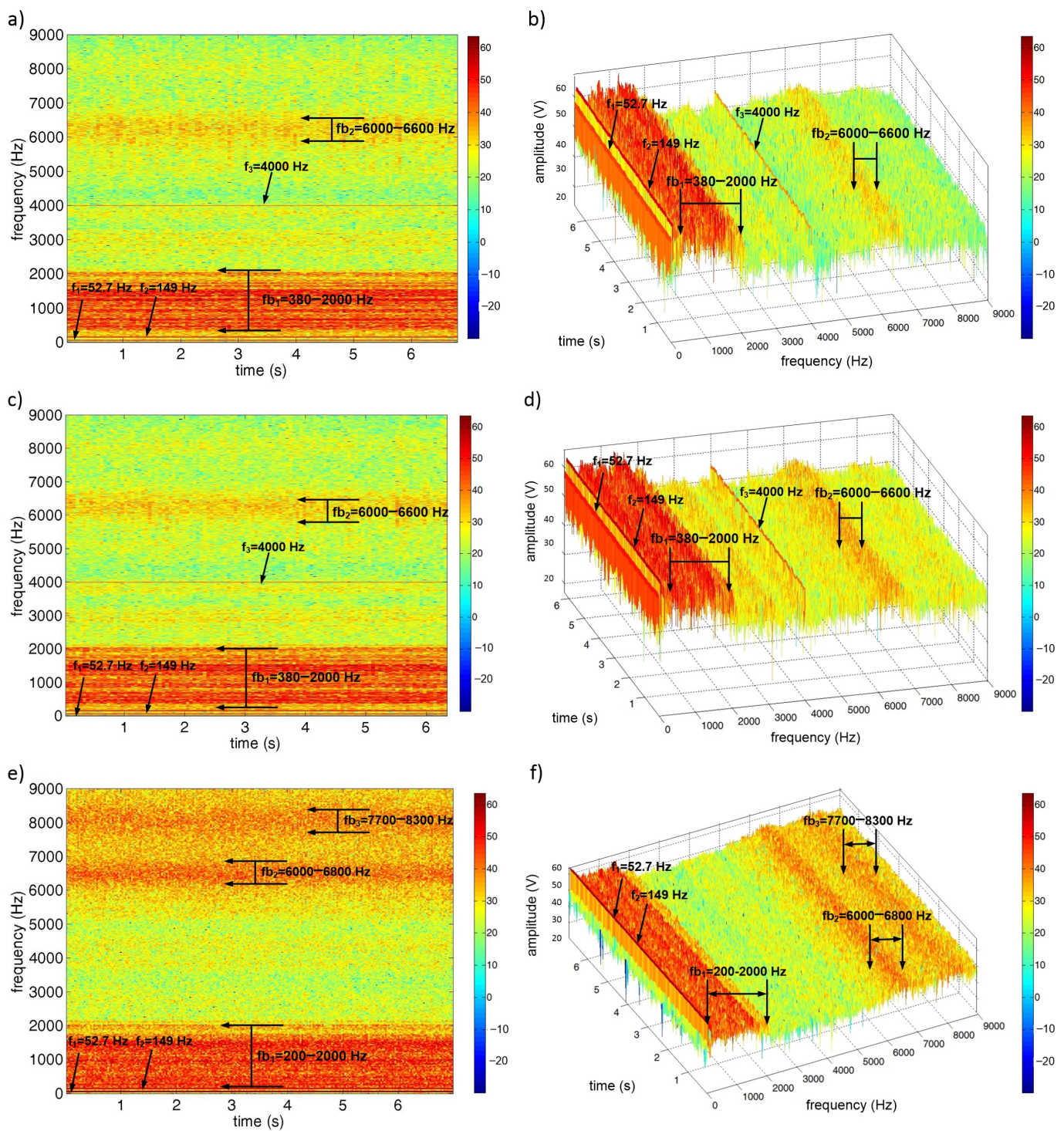


**Figure 15.** Spectrograms of vibration signals of acceleration ((a) three aggregates without drill bit—2D view, (b) three aggregates without drill bit—3D view, (c) three aggregates with drill bit—2D view, (d) three aggregates with drill bit—3D view, (e) andesite rock disintegration—2D view, (f) andesite rock disintegration—3D view).

### 5. Discussion and Future Work

Laboratory experimental measurements of the vibration signal of acceleration were carried out at two basic states of the device, namely during the operation of the device at no load and during the operation of the device when drilling andesite rock. Nine operating modes were measured within the adjustable states of the horizontal device.

The sources of vibrations in the rotary drilling environment are all aggregates and vibrations arising at the rock-drill bit interface. The very interaction of the drill bit as a tool with the rock is the largest source of vibration. It has negative effects on parts of the machinery. Therefore, identifying sources of vibration is important in minimizing side effects.

The process of rock disintegration and vibration generation is also affected by the properties of the drill bit, geomechanical properties of the rock being disintegrated (i.e., abrasiveness, grain size, hardness, strength, detachability), input values of pressure force  $F$  (N) and revolutions (rpm). Higher hardness, strength, grain, and other geomechanical properties cause stronger vibrations.

It can be stated that the vibrations generated by the device have the following components:

- vibrations of power units (i.e., motor, water pump, and hydro-generator);
- vibrations caused by contact between the drill bit and the rock;
- vibrations from the set values of pressure force  $F$  (N) and revolutions (rpm);
- vibrations due to the abrasiveness of the drilling tool during drilling;
- vibrations from the rinsing water inlet and outlet.

The results of the proposed signal processing methods can serve as inputs for recognition, vector quantization, and machine learning methods. In addition, the vibration signal processing in the time domain makes it possible to reliably determine specific characteristics and classify the signal according to the displayed waveform.

According to the time changes of the statistical characteristics, the vibrations have the character of a non-harmonic, periodic, quasi-periodic, and random signal. With periodic vibrations, the time waveform of the vibro-diagnostic acceleration variable is repeated. The generated vibrations are given by the superposition of compound and random vibrations. When processing vibration signals, the random component often overlaps a composite signal containing essential diagnostic information, a significant problem in industrial practice.

Time analysis is appropriate when there is a dominant vibration source; otherwise, diagnostic information is lost. Such a dominant vibration source is the motor unit on the drilling stand. However, the strong stochastic component of the signal caused by the transmission of vibrations from different areas of the machine complex can prevent the exact localization of the cause of the machine vibrations.

The total vibration of the machine is a measure of the energy associated with all the vibrations of the stand. The advantage of diagnosing the machine based on total vibrations is the speed and efficiency of the evaluation. The disadvantages of measuring total vibrations are the possibility of information loss in the noise.

Frequency analysis eliminates the disadvantages of analysis in the time domain locates the emerging failures of individual parts of the object. The amplitude spectrum and the power spectrum give the complete frequency analysis.

Dominant frequencies can be recognized from spectra and spectrograms. It can be stated that the individual operating modes have common frequencies of 52.73, 149.4, and 439.5 Hz in the lower frequency bands and differently in the middle band 1000–3000 Hz. A significant frequency is the value  $f = 4000$  Hz, which is in several operating modes. However, when drilling rock is andesite in IX. operating mode, this frequency is not recognized. There is a significantly specific higher frequency band 6000–9000 Hz.

Strategic is the three-dimensional representation of spectrograms, which allows us to study the dynamic time waveform of the vibrational signal in the time-frequency domain.

The motor combined with another unit, without or with a drill bit, has a fundamental effect on intense vibrations if we compare the proposed operating modes without direct drilling of andesite rock.

The greatest vibrations of the drilling equipment are caused by IX. operating mode, as the measured vibration signal includes higher frequencies, and andesite rock is disintegrated. The highest values of statistical characteristics in the time domain confirm the

correctness of the result of vibration signal processing and the conclusion regarding the IX. operating mode.

It is a view of signal processing and its presentation. However, if we look at applied research in terms of technical diagnostics of machines and equipment, it is complex technological machinery and a complex process of disintegration with many stochastic and non-linear elements.

When looking at the measured and processed vibration signals in more detail, it can be stated that the machine vibrations are closely related to the dynamic stress of the machine and the technical condition of individual shaft parts, spindles, unbalances of rotating parts, backlash in sliding sliders, wear of the drill bit, material fatigue. The vibrations of the rig are driven by both rotating and rectilinear moving parts, including the movement of the flushing fluid.

Practical experience confirms that the amplitude spectrum is used to detect the imbalance of the machine's rotating parts. For example, the headstock's misalignment with the drill bit is related to possible excessive wear.

The low-frequency range corresponds to the speed range of the headstock with the drill bit. The frequency spectrum is fundamentally non-harmonic, corresponding to the speed of the component. Other possible faults of the drilling equipment are the mechanical play of individual parts, damaged drive V-belts, defects on sliding sliders, and electrical or magnetic faults on electrical units.

The mid-frequency range corresponds to the frequency range of faults on electric motors. Therefore, spectral analysis of the vibration signal makes it possible to detect defects on the drilling stand such as wear of the contact surfaces of machine parts, ripping the diamond from the drill bit, and bending of the headstock with the drill bit, loosening of the drill bit.

The area of high and very high frequencies is characterized by surface fatigue of the diamond element material, chipping of the surface layer material, abrasiveness with an increase in play, and grooving on the sliders.

All these defects cause strong vibrations in the drilling equipment, which reduces the efficiency of the drilling process. Therefore, the primary goal of applied research and experimental laboratory measurements is vibration signal processing, identification of dominant frequencies, and fault localization. This will make it possible to innovate, reconstruct or replace faulty parts of the horizontal drilling stand.

Early machine fault diagnosis allows for early repair and replacement of damaged parts, thus preventing an accident or damage to the entire machine.

The following applied research will deal with the exact localization of defects on the drilling stand. Other methods for vibrational signal processing are also expected to be used, namely digital filtering, cepstral analysis, and wavelet transform. The research will also focus on developing new efficient methods for processing measured signals.

Methods of autocorrelation analysis, Fourier analysis, vector quantization, Statistical pattern recognition, and Canonical Discriminant Analysis (CDA) are used in the vibro-diagnostic analysis of machines and equipment in the articles, Principal Component Analysis (PCA), and others.

The methods presented in the article are essential for solving scientific problems in this area. The most significant problems include the recognition of drilled rock, diagnostics of worn and faulty parts of machinery, as well as preventive technical maintenance of machines [59–63].

## 6. Conclusions

Rotary rock disintegration is one of the basic and specific processes of geological and mining activities. Therefore, its research provides useful information that can be used in industrial practice, especially concerning efficiency, economy, and environmental performance in the context of optimization.

Equipment-generated vibrations have adverse effects on the drilling process, the drilling stand as a whole, and the individual aggregates.

Nevertheless, their measurement, monitoring, identification, and classification carry essential information about the disintegrating process. Measurements were performed at several selected operating modes.

This paper proposed methods for processing the vibration signal of acceleration that is generated during the operation of a laboratory horizontal drilling rig.

Because drilling and rig operation is random and non-linear, their research can be based on time-based statistical methods. In the time domain, significant results were achieved in the statistical characteristics, time waveform, and autocorrelation functions of the vibration signals of the respective modes.

In the frequency domain, research focused on the use of fast Fourier transform and the construction of signal amplitude and power spectra. As a result, dominant frequency components and bands have been identified.

The time-frequency domain showed the dynamic properties of individual aggregates and the whole process.

Based on the knowledge gained from the implementation of processing methods, it can be stated that the measured vibrational signals are deterministic, non-harmonic, and quasi-periodic, with a strong stochastic component and broad-spectrum.

A more rigorous evaluation of the vibration signal is very complicated because there is a superposition of several signal sources in the area of aggregates but also in the interaction of the drilling tool with the rock. Nevertheless, the presented research results show sufficient differences in autocorrelation functions, spectra, and spectrograms.

It is also possible to say that signal processing methods have been applied appropriately because the application of the process modeling principle is still unrealistic.

In addition to processing measured vibration signals, this paper also focused on determining the largest source of vibrations on the drilling stand. This source is the motor itself or in combination with other aggregates.

Due to the complexity of the horizontal laboratory drilling rig, further research will be needed in the field of signal processing and measurement methods, optimization, and modernization with subsequent reconstruction and innovation of the drilling stand. Therefore, the paper has a highly experimental character with an emphasis on applied research.

**Author Contributions:** Conceptualization, P.F. and J.K.; Data curation, P.F.; Formal analysis, P.F. and J.K.; Methodology, P.F. and M.D.; Project administration, J.K.; Resources, M.D. and M.L.; Supervision, M.D. and M.L.; Validation, J.K.; Writing—Original draft preparation, P.F. and J.K.; Writing—review and editing M.D. and M.L. All authors have read and agreed to the published version of the manuscript.

**Funding:** This research was funded by Slovak Research and Development Agency under contract Nos. APVV-18-0526, APVV-14-0892, and APVV-21-0027. The APC was funded by APVV-18-0526.

**Institutional Review Board Statement:** Not applicable.

**Informed Consent Statement:** Not applicable.

**Data Availability Statement:** No new data were created or analyzed in this study. Data sharing is not applicable to this article.

**Acknowledgments:** This work was supported by the Slovak Grant Agency for Science under grant VEGA 1/0289/22, and by the Slovak Research and Development Agency under contracts No. APVV-14-0892, APVV-18-0526, and APVV-21-0027.

**Conflicts of Interest:** The authors declare no conflict of interest.

## References

1. Krepelka, F.; Chlebová, Z.; Ivaničová, L. Measurement, analyzes and evaluation of stochastic processes operating in rock drilling. *Acta Mech. Slovak.* **2008**, *12*, 229–236.
2. Krepelka, F.; Chlebová, Z. Frequency analysis of the device acoustical response by rock drilling in connection with drilling process optimization. *Acta Mech. Slovak.* **2007**, *11*, 111–120.
3. Chlebová, Z. Simulation analysis of vibratory device controlled vibration. *Acta Mech. Slovak.* **2008**, *12*, 323–334.
4. Tiboni, M.; Remino, C.; Bussola, R.; Amici, C. A Review on Vibration-Based Condition Monitoring of Rotating Machinery. *Appl. Sci.* **2022**, *12*, 972. [[CrossRef](#)]
5. He, Z.; Cheng, W.; Xia, J.; Wen, W.; Li, M. Vibration source signal separation of rotating machinery equipment and robot bearings based on low rank constraint. *Appl. Sci.* **2021**, *11*, 5250. [[CrossRef](#)]
6. Kumar, S.; Loksha, M.; Kumar, K.; Srinivas, K. Vibration based Fault Diagnosis Techniques for Rotating Mechanical Components: Review Paper. *IOP Conf. Ser. Mater. Sci. Eng.* **2018**, *376*, 012109. [[CrossRef](#)]
7. Khoshouei, M.; Bagherpour, R. Predicting the Geomechanical Properties of Hard Rocks Using Analysis of the Acoustic and Vibration Signals During the Drilling Operation. *Geotech. Geol. Eng.* **2020**, *1*, 1573–1529. [[CrossRef](#)]
8. Botti, L.; Martin, B.; Barr, A.; Kapellusch, J.; Mora, C.; Rempel, D. R2: Drilling into concrete: Effect of feed force on handle vibration and productivity. *Int. J. Ind. Ergon.* **2020**, *80*, 103049. [[CrossRef](#)]
9. Flegner, P.; Kačur, J.; Durdán, M.; Leško, I.; Laciak, M. Measurement and processing of vibro-acoustic signal from the process of rock disintegration by rotary drilling. *Measurement* **2014**, *56*, 178–193. [[CrossRef](#)]
10. Wang, K.; Hu, Y.; Yang, K.; Qin, M.; Li, Y.; Liu, G.; Wang, G. Experimental evaluation of rock disintegration detection in drilling by a new acoustic sensor method. *J. Pet. Sci. Eng.* **2020**, *195*, 107853. [[CrossRef](#)]
11. Flegner, P.; Kačur, J.; Durdán, M.; Laciak, M. Processing a measured vibroacoustic signal for rock type recognition in rotary drilling technology. *Measurement* **2019**, *134*, 451–467. [[CrossRef](#)]
12. Flegner, P.; Kačur, J.; Durdán, M.; Laciak, M. Evaluating Noise Sources in a Working. *Pol. J. Environ. Stud.* **2019**, *28*, 3711–3720. [[CrossRef](#)]
13. Du, S.; Lv, J. Minimal Euclidean distance chart based on support vector regression for monitoring mean shifts of auto-correlated processes. *Int. J. Prod. Econ.* **2013**, *141*, 377–387. [[CrossRef](#)]
14. Trebuňa, F.; Šimčák, F.; Bocko, J.; Trebuňa, P. Failure analysis of mechanical elements in steelworks equipment by methods of experimental mechanics. *Eng. Fail. Anal.* **2010**, *17*, 787–801. [[CrossRef](#)]
15. Wittenberger, G.; Cehlár, M.; Jurkasová, Z. Deep hole drilling modern disintegration technologies in process of HDR technology. *Acta Montan. Slovaca* **2012**, *17*, 241–246.
16. Kahraman, S. Correlation of TBM and drilling machine performances with rock brittleness. *Eng. Geol.* **2002**, *65*, 269–283. [[CrossRef](#)]
17. Piltan, F.; Kim, J.M. Bearing anomaly recognition using an intelligent digital twin integrated with machine learning. *Appl. Sci.* **2021**, *11*, 4602. [[CrossRef](#)]
18. Cheng, L.; Lu, J.; Li, S.; Ding, R.; Xu, K.; Li, X. Fusion method and application of several source vibration fault signal spatio-temporal multi-correlation. *Appl. Sci.* **2021**, *11*, 4318. [[CrossRef](#)]
19. Zhu, D.C.; Zhang, Y.X.; Zhu, Q.W. Fault Diagnosis Method for Rolling Element Bearings Under Variable Speed Based on TKEO and Fast-SC. *J. Fail. Anal. Prev.* **2018**, *18*, 2–7. [[CrossRef](#)]
20. Li, J.W.; Fang, W.J.; Wan, L.; Liu, X.P.; Hu, W.D.; Cao, D.; Han, K.; Li, Y.Y.; Yan, Y.G. Research on the bonding properties of vitrified bonds with porous diamonds and the grinding performance of porous diamond abrasive tools. *Diam. Relat. Mater.* **2022**, *123*, 108841. [[CrossRef](#)]
21. Klaić, M.; Murat, Z.; Staroveski, T.; Brezak, D. Tool wear monitoring in rock drilling applications using vibration signals. *Wear* **2018**, *408–409*, 222–227. [[CrossRef](#)]
22. Maxit, L.; Karimi, M.; Guasch, O.; Michel, F. Numerical analysis of vibroacoustic beamforming gains for acoustic source detection inside a pipe conveying turbulent flow. *Mech. Syst. Signal Process.* **2022**, *171*, 108888. [[CrossRef](#)]
23. Qiu, H.; Yang, J.; Butt, S.; Zhong, J. Investigation on random vibration of a drillstring. *J. Sound Vib.* **2017**, *406*, 74–88. [[CrossRef](#)]
24. Qiu, H.; Yang, J.; Butt, S. Investigation on bit stick-slip vibration with random friction coefficients. *J. Pet. Sci. Eng.* **2018**, *164*, 127–139. [[CrossRef](#)]
25. Woodall, W.H.; Montgomery, D.C. Some current directions in the theory and application of statistical process monitoring. *J. Qual. Technol.* **2014**, *46*, 78–94. [[CrossRef](#)]
26. Xanthopoulos, P.; Razzaghi, T. A weighted support vector machine method for control chart pattern recognition. *Comput. Ind. Eng.* **2014**, *70*, 134–149. [[CrossRef](#)]
27. Kessai, I.; Benammar, S.; Doghmane, M.Z.; Tee, K.F. Drill bit deformations in rotary drilling systems under large-amplitude stick-slip vibrations. *Appl. Sci.* **2020**, *10*, 6523. [[CrossRef](#)]
28. Zurawski, M.; Zalewski, R. Damping of beam vibrations using tuned particles impact damper. *Appl. Sci.* **2020**, *10*, 6334. [[CrossRef](#)]
29. Barat, V.; Terentyev, D.; Bardakov, V.; Elizarov, S. Analytical modeling of acoustic emission signals in thin-walled objects. *Appl. Sci.* **2020**, *10*, 279. [[CrossRef](#)]

30. Kumar, R.; Kumaraswamidhas, L.; Murthy, V.; Vettivel, S. Experimental investigations on machine vibration in blast-hole drills and optimization of operating parameters. *Meas. J. Int. Meas. Confed.* **2019**, *145*, 803–819. [[CrossRef](#)]
31. Bian, J.; Ma, B.; Liu, X.; Qi, L. Experimental study of toolwear in electrochemical discharge machining. *Appl. Sci.* **2020**, *10*, 5039. [[CrossRef](#)]
32. Han, B.; Wang, S.; Zhu, Q.; Yang, X.; Li, Y. Intelligent fault diagnosis of rotating machinery using hierarchical Lempel-Ziv complexity. *Appl. Sci.* **2020**, *10*, 4221. [[CrossRef](#)]
33. *IEEE Std 181-2003*; IEEE Standard on Transitions, Pulses, and Related Waveforms. IEEE: Piscataway, NJ, USA, 2003; pp. 1–60. [[CrossRef](#)]
34. Balaji, M.; Venkata Rao, K.; Mohan Rao, N.; Murthy, B. Optimization of drilling parameters for drilling of Ti-6Al-4V based on surface roughness, flank wear and drill vibration. *Meas. J. Int. Meas. Confed.* **2018**, *114*, 332–339. [[CrossRef](#)]
35. Ghasemloonia, A.; Geoff Rideout, D.; Butt, S. A review of drillstring vibration modeling and suppression methods. *J. Pet. Sci. Eng.* **2015**, *131*, 150–164. [[CrossRef](#)]
36. Xiao, Y.; Hurich, C.; Butt, S. Assessment of rock-bit interaction and drilling performance using elastic waves propagated by the drilling system. *Int. J. Rock Mech. Min. Sci.* **2018**, *105*, 11–21. [[CrossRef](#)]
37. Xiao, Y.; Hurich, C.; Molgaard, J.; Butt, S. Investigation of active vibration drilling using acoustic emission and cutting size analysis. *J. Rock Mech. Geotech. Eng.* **2018**, *10*, 390–401. [[CrossRef](#)]
38. Prasad, B.; Babu, M. Correlation between vibration amplitude and tool wear in turning: Numerical and experimental analysis. *Eng. Sci. Technol. Int. J.* **2017**, *20*, 197–211. [[CrossRef](#)]
39. Pardo-Igúzquiza, E.; Rodríguez-Tovar, F.J. Spectral and cross-spectral analysis of uneven time series with the smoothed Lomb–Scargle periodogram and Monte Carlo evaluation of statistical significance. *Comput. Geosci.* **2012**, *49*, 207–216. [[CrossRef](#)]
40. Sierra-Alonso, E.; Caicedo-Acosta, J.; Gutiérrez, Á.; Quintero, H.; Castellanos-Dominguez, G. Short-time/-angle spectral analysis for vibration monitoring of bearing failures under variable speed. *Appl. Sci.* **2021**, *11*, 3369. [[CrossRef](#)]
41. Shim, J.; Kim, G.; Cho, B.; Koo, J. Application of vibration signal processing methods to detect and diagnose wheel flats in railway vehicles. *Appl. Sci.* **2021**, *11*, 2151. [[CrossRef](#)]
42. Krajňák, J.; Homišin, J.; Grega, R.; Kaššay, P.; Urbanský, M. The failures of flexible couplings due to self-heating by torsional vibrations—Validation on the heat generation in pneumatic flexible tuner of torsional vibrations. *Eng. Fail. Anal.* **2021**, *119*, 104977. [[CrossRef](#)]
43. Kaláb, Z.; Lyubushin, A. Power spectra of quarry blasting works measured in different depths. *Acta Mont. Slovaca* **2020**, *25*, 302–309. [[CrossRef](#)]
44. Yu, Y.; Qin, X.; Hussain, S.; Hou, W.; Weis, T. Pedestrian Counting Based on Piezoelectric Vibration Sensor. *Appl. Sci.* **2022**, *12*, 1920. [[CrossRef](#)]
45. Mirani, A.; Samuel, R. Discrete vibration stability analysis with hydromechanical specific energy. *J. Energy Resour. Technol. Trans. ASME* **2018**, *140*, 032904. [[CrossRef](#)]
46. Valíček, J.; Harničárová, M.; Kopal, I.; Palková, Z.; Kušnerová, M.; Panda, A.; Šepelák, V. Identification of upper and lower level yield strength in materials. *Materials* **2017**, *10*, 982. [[CrossRef](#)]
47. Panda, A.; Olejárová, Š.; Valíček, J.; Harničárová, M. Monitoring of the condition of turning machine bearing housing through vibrations. *Int. J. Adv. Manuf. Technol.* **2018**, *97*, 401–411. [[CrossRef](#)]
48. Nahorni, V.; Panda, A.; Valíček, J.; Harničárová, M.; Kušnerová, M.; Pandová, I.; Legutko, S.; Palková, Z.; Lukáč, O. Method of Using the Correlation between the Surface Roughness of Metallic Materials and the Sound Generated during the Controlled Machining Process. *Materials* **2022**, *15*, 823. [[CrossRef](#)]
49. Lednická, M.; Kaláb, Z. Vibration Effect of Near Earthquakes at Different Depths in a Shallow Medieval Mine. *Acta Geophys.* **2016**, *64*, 2244–2263. [[CrossRef](#)]
50. Shreedharan, S.; Hegde, C.; Sharma, S.; Vardhan, H. Acoustic fingerprinting for rock identification during drilling. *Int. J. Min. Miner. Eng.* **2014**, *5*, 89–105. [[CrossRef](#)]
51. Masood.; Vardhan, H.; Aruna, M.; Rajesh Kumar, B. A critical review on estimation of rock properties using sound levels produced during rotary drilling. *Int. J. Earth Sci. Eng.* **2012**, *5*, 1809–1814.
52. Chongfuangprinya, P.; Kim, S.B.; Park, S.K.; Sukchotrat, T. Integration of support vector machines and control charts for multivariate process monitoring. *J. Stat. Comput. Simul.* **2011**, *81*, 1157–1173. [[CrossRef](#)]
53. Khoshouei, M.; Bagherpour, R.; Jalalian, M. Rock Type Identification Using Analysis of the Acoustic Signal Frequency Contents Propagated While Drilling Operation. *Geotech. Geol. Eng.* **2021**, *1*, 1–14. [[CrossRef](#)]
54. Kahraman, S.; Delibalta, M.; Comakli, R.; Grafov, B. Noise level measurement test to predict the abrasion resistance of rock aggregates. *Fluct. Noise Lett.* **2013**, *12*, 1350021. [[CrossRef](#)]
55. Zhao, X.X.; Gong, Y.D. Research on the Load on Cutter Head of Hard Rock Tunnel Boring Machine. *Appl. Mech. Mater.* **2014**, *684*, 303–307. [[CrossRef](#)]
56. Krishnakumar, P.; Rameshkumar, K.; Ramachandran, K. Tool wear condition prediction using vibration signals in high speed machining (HSM) of Titanium (Ti-6Al-4V) alloy. *Procedia Comput. Sci.* **2015**, *50*, 270–275. [[CrossRef](#)]
57. Smulko, J.; Kish, L. High-order statistics for fluctuation-enhanced gas sensing. *Sens. Mater.* **2004**, *16*, 291–299.
58. Lentka, L.; Smulko, J.; Kotarski, M.; Granqvist, C.; Ionescu, R. Non-gaussian resistance fluctuations in gold-nanoparticle-based gas sensors: An appraisal of different evaluation techniques. *Sensors* **2017**, *17*, 757. [[CrossRef](#)]

59. Shan, X.; Tang, L.; Wen, H.; Martinek, R.; Smulko, J. Analysis of vibration and acoustic signals for noncontact measurement of engine rotation speed. *Sensors* **2020**, *20*, 683. [[CrossRef](#)]
60. Puchalski, A. A technique for the vibration signal analysis in vehicle diagnostics. *Mech. Syst. Signal Process.* **2015**, *56*, 173–180. [[CrossRef](#)]
61. Bartelmus, W.; Zimroz, R. A new feature for monitoring the condition of gearboxes in non-stationary operating conditions. *Mech. Syst. Signal Process.* **2009**, *23*, 1528–1534. [[CrossRef](#)]
62. Osburn, A.; Kostek, T.; Franchek, M. Residual generation and statistical pattern recognition for engine misfire diagnostics. *Mech. Syst. Signal Process.* **2006**, *20*, 2232–2258. [[CrossRef](#)]
63. Zimroz, R.; Bartkowiak, A. Two simple multivariate procedures for monitoring planetary gearboxes in non-stationary operating conditions. *Mech. Syst. Signal Process.* **2013**, *38*, 237–247. [[CrossRef](#)]